Journal of Engineering Mathematics **43:** 315–346, 2002.

Swirl-flow effects in a duct bending through a substantial angle

F.T. SMITH and L. LI
Department of Mathematics, University College London, Gower Street, London WC1E 6BT, U.K.

Received 7 March 2001; accepted in revised form 15 November 2001

Abstract. The vortical three-dimensional flow of an inviscid incompressible fluid through a bend in a slender duct is investigated with nonlinear coupling between the centre-line and cross-sectional velocities. The bend, although gradual, turns the duct flow through a finite angle typically. The theoretical work is motivated directly by the industrial application to food sorting, involving the rapid firing of impulsive ejectors and sprinklers which combine short time scales and flow turbulence, and indirectly by other applications. The flow response depends largely on the relative radius of curvature in the bend along with the cross-sectional swirl and the shear in the perturbed streamwise velocity profile at the entrance. Solutions for the motion within and beyond the bend are determined computationally through a fourth-order compact scheme, for both rectangular and smooth cross-sections, and analytically for a general cross-section, under varying entrance conditions (especially for increasing swirl there, although a long bend for example also enhances swirl downstream). The total streamwise vorticity is found analytically to increase in direct proportion to the distance along the bend, whether the inertial effects are weak or strong. The smallness of the pressure loss also contrasts with that in viscous flows.

Key words: bends, ducts, food, sorting, swirl.

1. Introduction

The present study arose directly from numerous contacts with, and work done for, the food-sorting industry. There is particular industrial and theoretical interest here in the performance of impulsive ejectors using a pressure supply to force fluid quickly through a bend in a duct. The research undoubtedly has wider industrial interest also.

Bends in ducts, pipes, arteries and other internal shapes are common, arising either through necessity in manufacturing or through nature, in industrial flow applications, plumbing, machinery dynamics and physiological flows. In practice, three-dimensional ducts for example often involve quite basic cross sections which are rectangular or circular for the sake of ease and reasonable precision in manufacture, rectangles in particular being used widely in heat and mass-transfer devices. The bends in ducts are often quite slender, but turn the duct centre line through a significant angle. Many of the flows produced through such bends are turbulent and/or unsteady; one such form arises in the rapid firing of impulsive ejectors and sprinklers where a high-pressure supply is used to force fluid at quite high speed through a bent duct over a relatively short time interval, and a not too dissimilar process occurs in pulsating blood motion into and through the aortic arch. The characteristic Reynolds numbers are large and the bends generally are, in practical terms, the sources of substantial losses in pressure head and of related complications concerning enhanced secondary motions, due to centrifuging, while on the theoretical side they tend to restrict or negate the use of traditional inviscid one-dimensional duct-flow analysis for an entire duct. The important typical bend-flow properties in reality thus involve

(a) basic cross sections, *e.g.* rectangular;

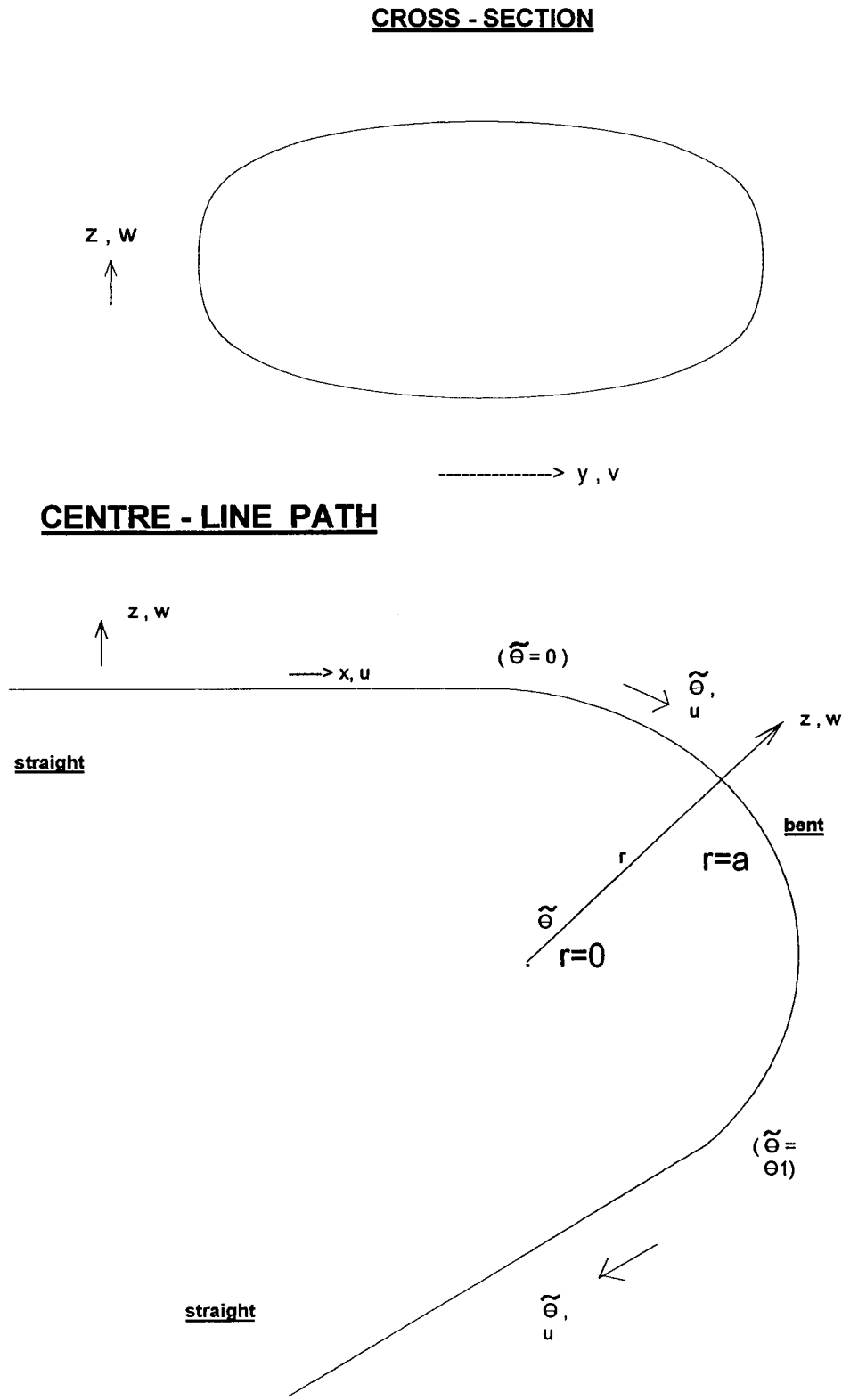

Figure 1. Sketch of the bent duct flow configuration (a) Cross-section in y, z (arbitrary). (b) Centre-line path, with θ_1 being finite.

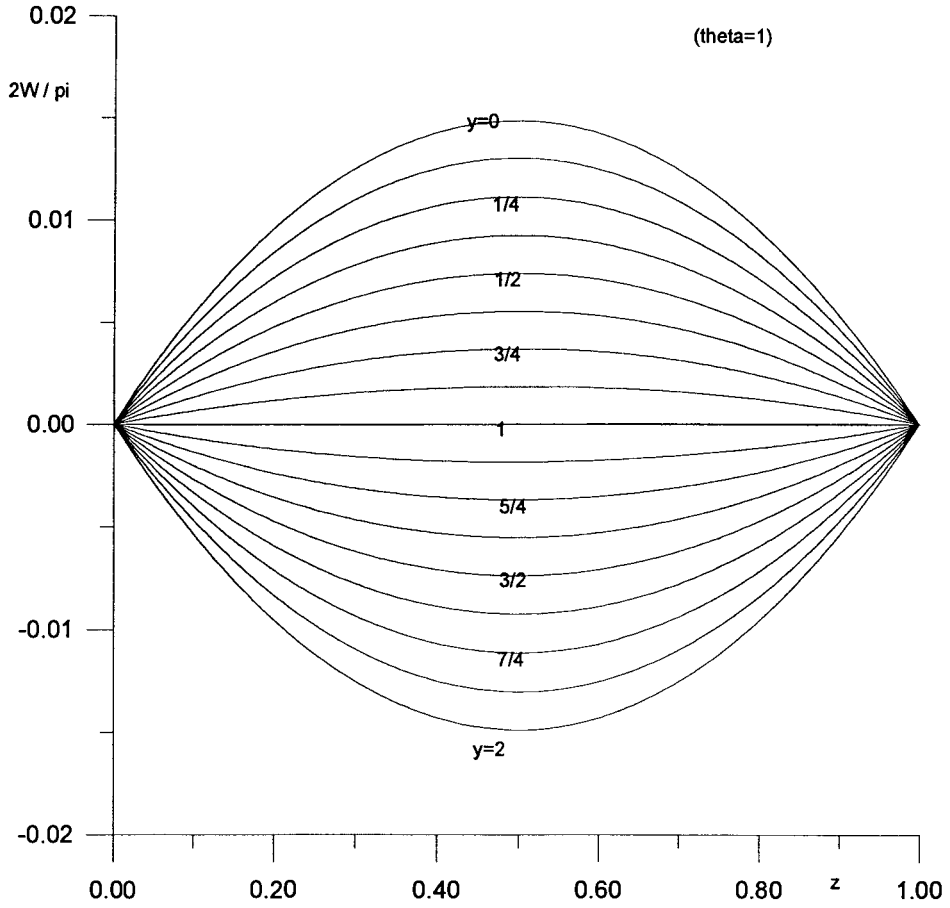

Figure 2. Rectangular cross section. Computational results for the entrance condition (3.4) on $[U_I, V_I, W_I]$ at $\theta = 0$, with $c = 0{\cdot}01(\pi/2)^2$, and comparison with the analytical result from (4.2). (a) and (b): cross-plane velocity profiles at $\theta = 1$. (c): streamwise vorticity at $\theta = 1$. (d): $2W/\pi$ along $(y, z) = (0, \frac{1}{2})$ versus $\pi\theta/2$, from a coarse grid computation (lower curve) and analysis (upper curve), within and after the bend.

(b) turning through a finite angle;
(c) turbulent flow;
(d) unsteady motion;
(e) large flow rates.

The point (c) is due to valves or imperfections upstream, or to the duct walls not being perfectly smooth because of manufacturing considerations. The same points (a)–(e) apply in many industrial settings as well as that of food sorting where the necessary supply of fast moving fluid cannot be achieved by means of an ideal smooth-walled straight vessel, often because of spatial as well as duct-manufacture constraints. Added to this are complications from multi-component devices, complex geometry and multiple firing over an extremely short time period.

For the three-dimensional bent-duct flows above, *i.e.* practical industrial ones involving all or part of the aspects (a)–(e), understanding and prediction seem to consist mostly of interesting empirical results for the losses and occasional remarks on secondary flows: see in [1–4].

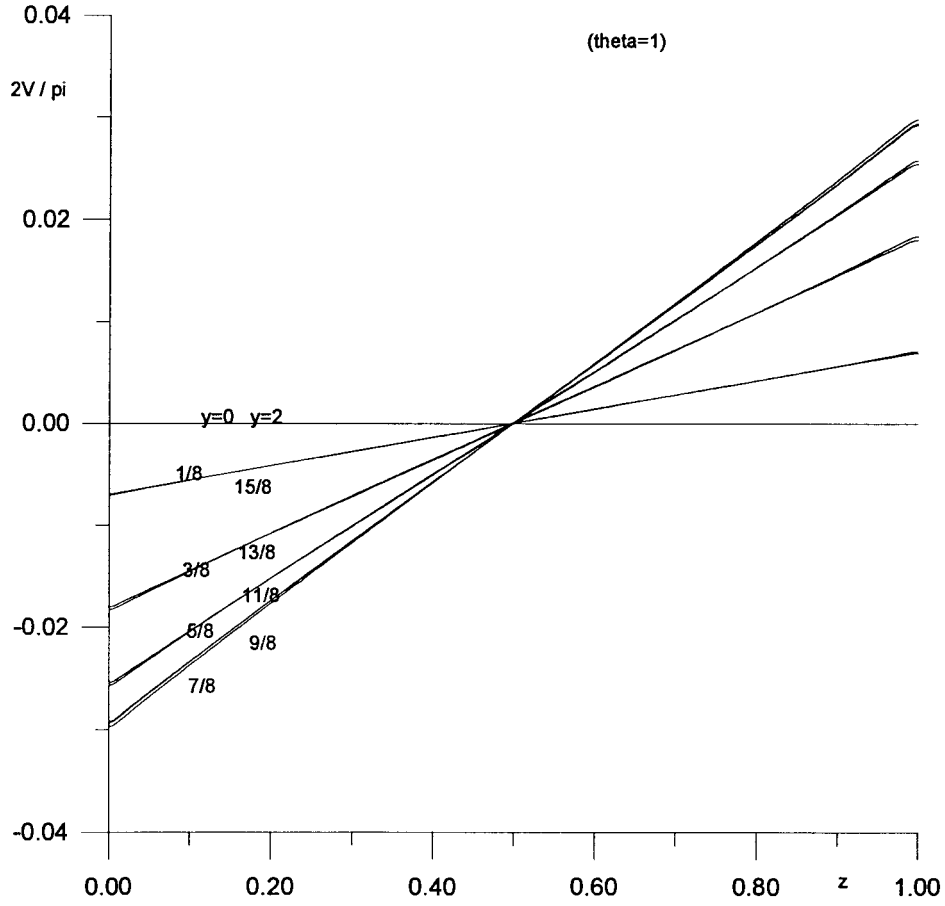

Figure 2. Continued.

By contrast there has been much theoretical study on laminar, viscous, developing or fully developed, steady flow through a bent pipe rather than the cases surrounding (a)–(e) of interest to industry. Fully developed motions were considered by Dean [5] and many others including [6–12]. Developing entry motions were studied either for a uniform entry velocity profile, as in [13, 14] and many references therein, or for a sheared profile with no slip at the walls, as in [15, 16] and references therein. Unsteady flows have also been investigated along similar lines, for example by [11, 17]. See also in [18], [19, Chapter 5], [20], a recent experimental and computational study of swirling flow in a graft in [21], and a review by [22]. Two-dimensional bends are considered by [23–29], covering computations, experiments and theory.

The current focus is different from that of the Dean-type problems, however. The largeness of the typical Reynolds number coupled with the short time scale and likely turbulence in the duct-flow applications described earlier (indeed all of (a)–(e)) tend to call for a nonlinear inviscid treatment rather than, or complementary to, the majority of those in the preceding paragraph. The present treatment is associated with plug flow in the turbulent case and with the property of attached flow persisting for a finite scaled time in the laminar case. Indeed in the unsteady case where virtually inviscid flow is set up almost immediately the viscous thickness of the Rayleigh layer increases only as the square root of ⟨kinematic viscosity multiplied by time⟩, which remains comparatively small for many common fluids over short

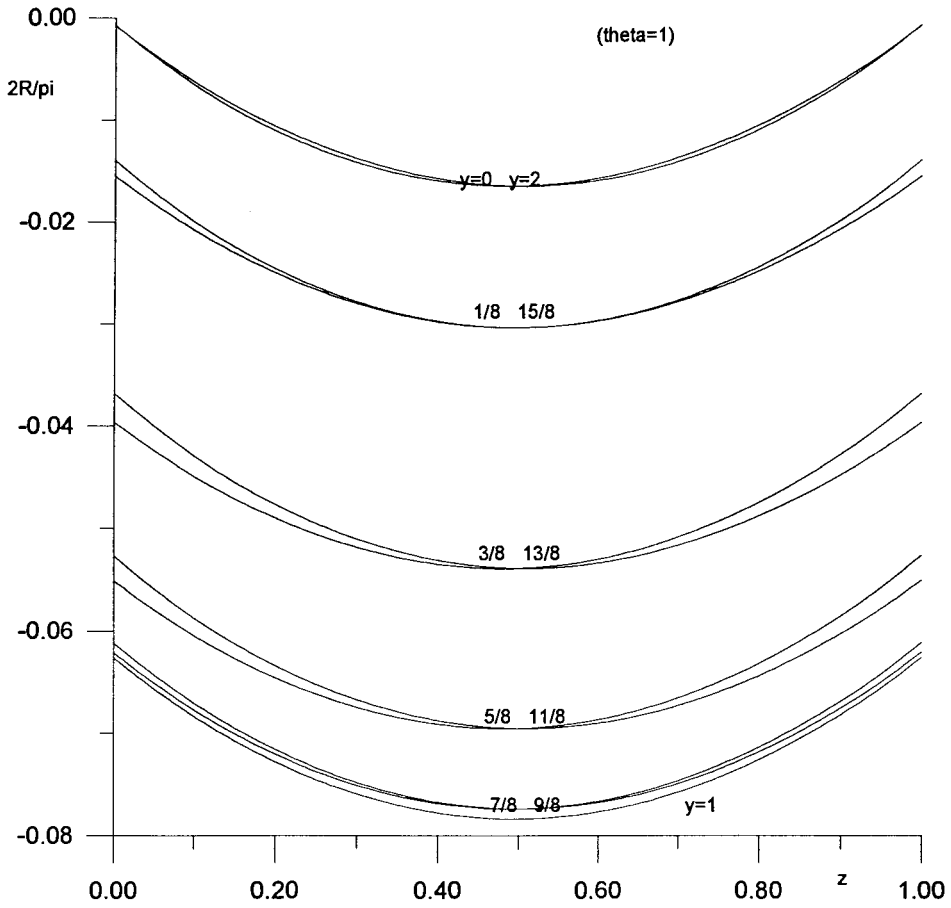

Figure 2. Continued.

time scales. The industrial and other applications also point to the inclusion in the theory of finite angles of flow turning produced by the three-dimensional bend. Hence herein we assume an inviscid nonlinear response together with a slightly disturbed uni-directional incident flow entering a sizeable bend of simple cross section; these assumptions are all in line with the practical aspects (a)–(e) stressed at the outset. Likewise the impact on one-dimensional analysis requires consideration, given the potentially substantial effects of swirl on the centre-line velocity within the bend and the question of its influence or decay downstream of the bend. These issues, which are supplemented by complex aspects of compressibility in those of the real applications that involve gas dynamics, form the background for the current study, which is for an incompressible fluid.

The nonlinear inviscid-flow theory taking account of (a)–(e) above is a main new feature here, combined with an investigation of incident swirl effects both numerically and analytically and with the capability of extending classical compressible duct-flow theory to allow for bends.

Section 2 describes the configuration and assumptions in detail for the inviscid motion ahead of, inside, and beyond the bend in a duct. The duct and bend are taken to be slender but producing in the typical case a finite turning angle, for example 90°, in total, and any unsteady effects are confined to thin negligible wall layers The nonlinearly coupled flow through the

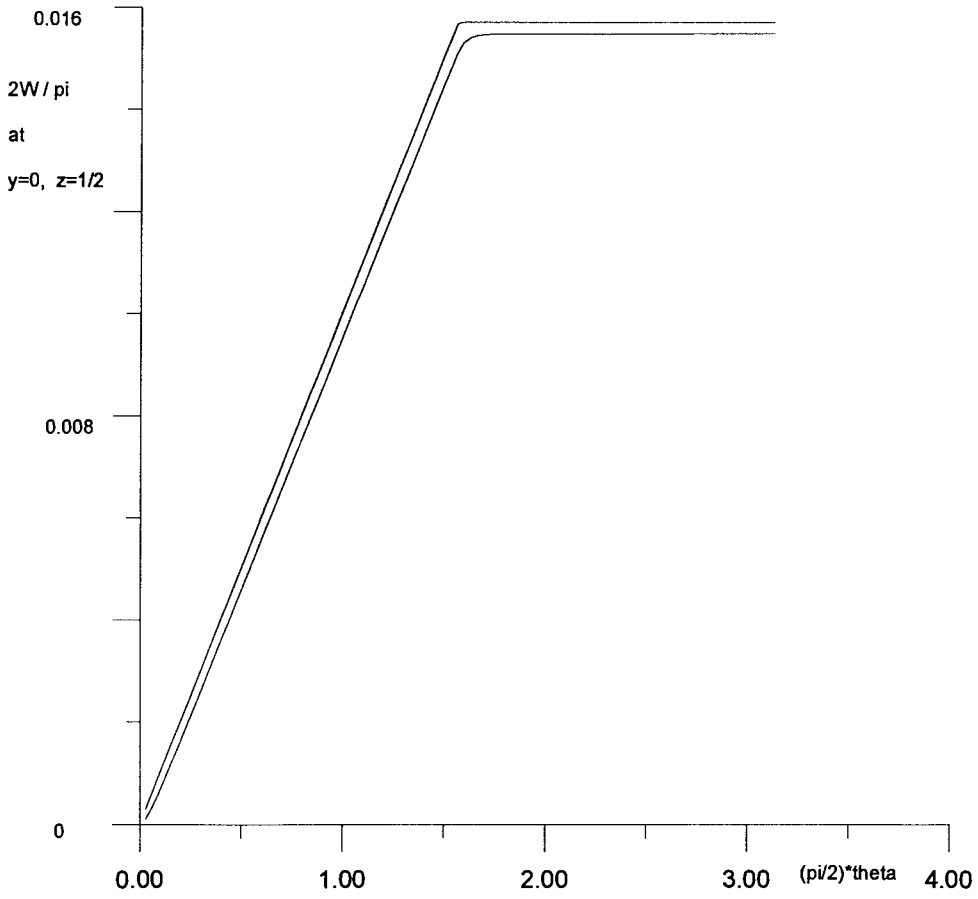

Figure 2. Continued.

bend is most dependent on the input swirl in the cross-sectional plane and the shearing in the streamwise perturbation velocity profile at the bend entrance; see also [22]. In industrial settings this input swirl and shearing are provoked by conditions further upstream due for example to a valve, surface roughness or another bend, and the swirl and shearing combine with the bend curvature to form the main parameters, which for a given turning angle are the relative shearing velocity multiplied by the relative radius of curvature and the comparative strength of the swirling flow. Computational compact-differencing and analytical properties are discussed in Sections 3 and 4–5 in turn, the former being for rectangular and other, smooth, cross sections and the analytical findings applying mostly for a general bounded cross section. A linear increase which is found numerically and confirmed analytically in the integrated streamwise vorticity with increasing distance around the bend is the major general effect from the centrifuging in the bend, an effect which controls the downstream flow for weak or strong nonlinearity within the bend. Further points are presented in Section 6, in particular on the reduction in pressure response and the accentuation of secondary flow swirl in the bend.

2. The bent-flow configuration

The duct of concern here is straight in its upstream section, then bent in the middle and followed by a straight section downstream as shown in Figure 1. The total angle thus turned through is denoted by θ_1. The coordinates x, in the direction of the duct axis, and y, z, perpendicular to that axis, are nondimensionalized with respect to a typical cross-sectional distance h_D of the upstream duct, while the corresponding nondimensional velocity components u, v, w are measured relative to the upstream incident nearly uniform axial flow speed u_D at the onset of the bend. The pressure variation p is based on $\rho_D u_D^2$ where ρ_D is the density of the fluid, which is taken to be inviscid and incompressible. The radius a_D of curvature of the duct centreline in the bent section is assumed to be constant and large compared with h_D, giving a large ratio $a_D/h_D \equiv a$. Again, the incident motion is nearly uniform and nearly unidirectional (*i.e.* nearly standard inviscid flow) in the sense that the streamwise (axial) velocity u is unity to within an order ϵ which is small and the cross-sectional velocity components v, w are also small. The aim is to determine the three-dimensional steady flow through the bend and beyond.

The assumptions taken here, then, are in summary that the motion is steady, inviscid and incompressible, with almost unidirectional incident flow ahead of the slender substantial bend of simple cross section. These allow for the points (a)–(e) listed in the introduction.

For the flow in the bend cylindrical polar coordinates $r, \tilde{\theta}, y$ may be used as defined in Figure 1, with corresponding velocity components w, u, v again. Here $r = a + z$ with z typically of order unity and $\tilde{\theta}$ is equivalent to x/a and is guessed to be also of order unity if the total angle θ_1 is substantial. Continuity would suggest that v, w are then of order a^{-1} at most, yielding a radial inertial force ($\sim v\partial w/\partial y,\ w\partial w/\partial r$) proportional to a^{-2}, whereas the centrifugal force ($\propto -u^2/r$) which represents the main effect of the bend is larger, as it is proportional to a^{-1}.

The role of the shear in the streamwise velocity is important here, combined with the entrance swirl. The reason is that the centrifugal force can be balanced simply by the radial pressure gradient if for instance the streamwise velocity has no incident dependence on the cross-plane coordinate y normal to the radius. This allows a flow solution in which the streamwise velocity u depends only on $\tilde{\theta}$, the streamwise pressure gradient is $-u\,u'$, the pressure correction is in effect $a^{-1}u^2 z$ and u is determined by the conservation of mass, essentially u multiplied by the cross-sectional area of the bent duct. Thus the flow then remains quasi-one-dimensional and the bend has no major effect. A similar conclusion holds if u depends only on $z, \tilde{\theta}$. In contrast, if there is strong vorticity/shear such that u depends nontrivially on the radial and normal-radial distances z, y as well as $\tilde{\theta}$, then the above centrifuging radial pressure variation also sets up a comparable pressure variation in the normal-radial y direction and hence through inertia larger cross-plane velocities v, w than expected. These, in turn, indicate a probably shorter scale in $\tilde{\theta}$ for continuity and overall the influence of the bend can be much stronger.

Here, to account for the above contrast, we take an intermediate case of low swirl and relatively small radial and normal-radial dependence in the streamwise velocity u, throughout, in the sense that $(u - 1, v, w)$ is

$$\epsilon(\tilde{U}, \tilde{V}, \tilde{W})$$

with the given factor ϵ being small. The factor ϵ represents broadly the comparative strength of the incident streamwise shear and cross-section swirl, while $\tilde{U}, \tilde{V}, \tilde{W}$ are of typical order

unity and depend on $\tilde{\theta}, y, z$. This form for the velocity is accompanied by a pressure p variation $\epsilon\tilde{p}_0(\tilde{\theta}) + z/a - z^2/(2a^2) + \epsilon^2\tilde{p}_1(\tilde{\theta}, y, z)$ in the bend. The parameter ϵa is denoted by α below and is taken to be of order one. Also to normalize we set

$$[\tilde{U} + \alpha^{-1}\Gamma z, \tilde{V}, \tilde{W}] = \alpha^{-1}\theta_1^{-2}[U, \theta_1 V, \theta_1 W], \quad \tilde{\theta} = \theta_1\theta,$$

together with $\alpha\theta_1^2\tilde{p}_0 = p_0$, $\alpha^2\theta_1^2\tilde{p}_1 = p_1 - \Gamma\theta_1^2 z^2$ and Γ is zero or unity as specified just below. Then the equations of continuity and momentum reduce to

$$V_y + W_z = 0, \tag{2.1a}$$

$$U_\theta + VU_y + WU_z = -p_0'(\theta), \tag{2.1b}$$

$$V_\theta + VV_y + WV_z = -p_{1y}, \tag{2.1c}$$

$$W_\theta + VW_y + WW_z - 2\Gamma U = -p_{1z}. \tag{2.1d}$$

In the straight sections ($\theta < 0$, $\theta > 1$) of the duct, Γ is identically zero in effect. Indeed, ahead of the bend one acceptable flow solution has V, W, p_1 all zero, with U dependent only on θ and $U + p_0$ constant, a solution which represents unidirectional incident motion. This is a standard feature of straight inviscid duct flows. Other incident flows are possible, nevertheless, with swirl such that V, W are nonzero and the evolution of the latter components is decoupled from that of the streamwise velocity, within a straight section. In the bent section ($0 < \theta < 1$) of duct, on the other hand, Γ is identically one.

The flow solution has parabolic dependence on θ, which clearly acts as a time-like variable in (2.1b–d), but there is essentially elliptic dependence in the y, z cross-plane. The starting condition at the entry to the bend is taken to be

$$[U, V, W] = [U_I, V_I, W_I](y, z) \quad \text{at} \quad \theta = 0 \tag{2.2a-c}$$

where the scaled velocity components on the right-hand side are given from the incident straight-duct flow described earlier and are generally of order one. Although the parameters α, θ_1 provide some measure of the strength of the bend effect, the comparative values and forms of the swirl components V_I, W_I are also important as we will see. Their relationship to the original velocity components is $(U_I, V_I, W_I) \equiv \alpha\theta_1(\theta_1\tilde{U}_I + \alpha^{-1}\Gamma z\theta_1, \tilde{V}_I, \tilde{W}_I)$ and is worth recording here. Our primary concern will be with the influences of the swirl components, particularly in view of the practical applications, whereas those of the other parameters will be addressed afterwards in Section 6. The boundary conditions at each θ station read

$$\psi = 0 \text{ at the duct boundary,} \tag{2.3a}$$

$$\iint U \, \mathrm{d}y \, \mathrm{d}z = \text{constant (for all } \theta). \tag{2.3b}$$

Here (2.3a) stems from use of the scaled stream function ψ such that

$$V = -\psi_z, \qquad W = \psi_y, \tag{2.4}$$

in view of (2.1a) which implies mass conservation for the cross-plane flow. Condition (2.3b) also comes from the continuity balance, but at higher order, applied in integrated form over the whole cross section at each θ station.

The flow in the bend and downstream of it is therefore governed by the coupled Euler-like system (2.1a–d) subject to (2.2a)–(2.4). There is no upstream influence at this level of working and in principle a forward march in θ should give the flow solution for any prescribed θ_1, α value with the entrance conditions (2.2a–c) prescribed.

3. Computational study

Numerical solutions were computed for the case of a constant rectangular cross-section first, given by y, z ranging from 0 to y_1, 0 to z_1, respectively, and prescribed constants y_1, z_1, for all θ. The numerical method used for tackling the governing equations is based on solving the streamwise-vorticity equation

$$R_\theta + VR_y + WR_z = 2\Gamma U_y \tag{3.1}$$

combined with (2.1b), (2.4). Here (3.1) follows from eliminating p_1 between (2.1c,d) and setting

$$R = \nabla^2 \psi \tag{3.2}$$

with ∇^2 denoting the Laplacian operator $\partial^2/\partial y^2 + \partial^2/\partial z^2$. The solution is forward marched in θ from given conditions at $\theta = 0$. If to begin with we consider straightforward backward differencing being applied to the θ derivatives in (2.1b), (3.1) then, in (3.1) for example, $\partial R/\partial\theta$ is replaced simply by $(R_{n+1} - R_n)/\Delta\theta$. Here the subscript n denotes quantities at the successive discretized θ values, separated by a small step $\Delta\theta$, and R_n is known, whereas all other terms are taken as unknowns at the θ level $(n + 1)$.

Discretized versions of the governing equations are then solved iteratively for the $(n + 1)$-level variables, using (2.1b) to obtain all the new U_{n+1} values for given V_{n+1}, W_{n+1}, then (3.1) for all the R_{n+1}, (3.2) with (2.3a) for the ψ_{n+1}, (2.4) to update all V_{n+1}, W_{n+1} values, and then re-solving for U_{n+1} and so on. The iterations are continued until the nonlinear discrete system produces convergence. With derivatives in y, z treated by compact differencing (see [30–32] and (3.3a–c) below), the Equations (2.1b), (3.1), (3.2) are solved through multiple sweeping line-by-line across in y from 0 to y_1. It was soon found that, for (2.3b) to be satisfied, p_0 must be identically zero, as confirmed in the next section, and that property reduced the number of iterations required. In the compact differencing approach, for the U equation the inertial term $V\partial U/\partial y + W\partial U/\partial z$ is written in conservative form as $P + Q$ where, in view of (2.1a), $P \equiv \partial(VU)/\partial y$, a relation which is discretized as

$$\sum_{\ell=1}^{3} \{g_\ell P_\ell - \tilde{g}_\ell V_\ell U_\ell/\Delta y\} = 0, \tag{3.3a}$$

and similarly for $Q \equiv \partial(WU)/\partial z$. The latter is discretized in the form

$$\sum_{m=1}^{3} \{g_m Q_m - \tilde{g}_m W_m U_m/\Delta z\} = 0. \tag{3.3b}$$

These discretizations are combined with the implied U-P-Q relation, which is

$$(U_{n+1} - U_n)/\Delta\theta + P + Q = 0. \tag{3.3c}$$

In (3.3a,b) the coefficients $g_1, g_2, g_3, \tilde{g}_1, \tilde{g}_2, \tilde{g}_3$ are $\frac{1}{3}, \frac{4}{3}, \frac{1}{3}, -1, 0, 1$, respectively, and the subscript $\ell = 1, 2, 3$ denotes values at three representative successive positions in the y direction separated by a small step length Δy, to give fourth-order spatial accuracy, and likewise for $m = 1, 2, 3$ in z with a small step Δz, whereas (3.3c) is applied at every single point. The same treatment is applied to the R equation and likewise for derivatives in the R-ψ equation and in updating V, W. Fine grids were necessary to avoid significant oscillations as the strength of the entrance flow was increased, particularly for increasing θ. Upwind differencing was also applied to the y, z derivatives in (2.1b), (3.1) to account for sign changes in V, W and this proved more stable though less accurate generally. Comparisons with results from a more standard second-order approach were found to be supportive of the accuracy of the fourth-order method (and we remark that the latter works far better in the present context, where viscous smoothing is absent). In addition, the above backward differencing in θ was in practice made second-order accurate by taking half steps in θ and averaging.

Typical grids used had 120 by 120 points in the cross-section, a step length 0·0005 to 0·002 in θ and 10–50 iterations per step. Refinement was required for the more severe cases described later. Comparisons were made on different grids, suggesting an error estimate of well below 1% in general. In some cases refined grid calculations required rather fewer iterations. The scheme was marched forward in θ through the bend from zero to 1 with Γ equal to unity and then from 1 onwards Γ was set to zero for the downstream section of the duct.

Results were obtained for various entrance conditions (2.2a–c) and values of the parameters α, θ_1. For now we concentrate on a 2 by 1 rectangle, so that $y_1 = 2, z_1 = 1$. The results presented are in Figures 2–5, for the two forms of input condition $[U_I, V_I, W_I]$ given by

$$2c[y^3/3 - y^2 + z^2 y - zy,\ 0,\ 0], \tag{3.4}$$

$$\frac{2}{5\pi}\left[c_1 \sin y,\ -2c_2 \sin\left(\frac{\pi y}{2}\right)\cos(\pi z),\ \ c_2 \cos\left(\frac{\pi y}{2}\right)\sin(\pi z)\right], \tag{3.5}$$

partly to provide an inkling of generality. Here c, c_1, c_2 are prescribed constants, with $|c_2|$ giving the maximum amplitudes of the scaled streamwise vorticity R at the entrance. Figure 2 is concerned with (3.4) at a low value of c, while Figures 3–5 show results for the entrance form (3.5) with c_1 fixed at $\pi^3/16$ for a range of values of the input swirl constant c_2. Comparisons are presented or noted with the analytical work of the following sections. It is interesting also to note the evolution of V, W to a new steady state beyond the bend (where Γ is zero) and the separate evolution of the U field there.

In more detail, Figure 2(a–d) shows the velocity components V, W and vorticity R obtained at the end of the bend, followed by the axial development of the value of W midway along the left side of the duct according to the computational solution and to (4.2) below. The agreement is close. Figure 2(b,c) indicates the slight off-symmetry at this zero level of swirl. Figure 3(a–c), which is likewise for zero input swirl but a different U_I profile, also indicates small effects appearing by the end of the bend and beyond, although the U profiles in Figure 3(a) are significantly inclined compared with the horizontal input profiles. In Figure 3(c), and subsequently, D denotes the computed double integral of R with respect to y, z over the cross section; see the left-hand side of (4.5) below, while the linear prediction from the right-hand side also agrees with these computations. The rest of the axial development shown in Figure 3(c) is in line with (4.1) below and with Figure 2. Figure 4(a–d), for increased (nonlinear) input swirl velocities, shows more distorted profiles of U, V, W, R at

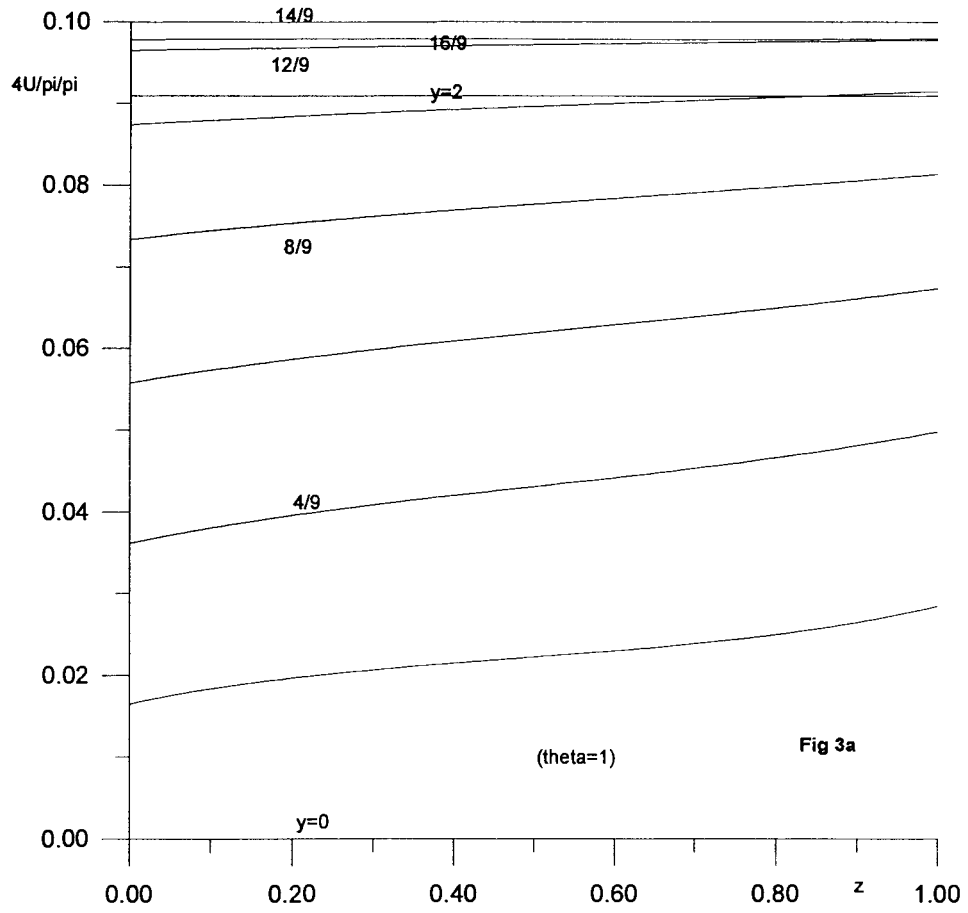

Figure 3. Rectangular section. Solutions for input (3.5) with $c_1 = \pi^3/16$, swirl parameter $c_2 = 0$. (a) $4U/\pi^2$ profiles at $\theta = 1$. (b) $2V/\pi$, $2W/\pi$ profiles at $\theta = 1$, $\theta = 3/2$. (c) gives D and V, W along different cross-plane positions, versus $\pi\theta/2$; D is the integral of R over the duct cross-section at any θ station.

the end of the bend and beyond. In Figure 4(a,b) the average of the maximum V, W values is about 3 times the maximum U value, while the R profiles in Figure 4(c) imply substantial rotation due to the increased helical motion. In addition, strong variation near the duct edges becomes apparent in Figure 4(a), especially at and near $y = 0$, and indeed grid refinement pointed to strong variation of R near the corners: see Figure 4(c). Here again the axial dependence of D in Figure 4(d) suggests linear behaviour. Figure 5(a–d) is for even larger input swirl. Much more pronounced contortion of the U profiles occurs now (Figure 5(a)) but the U values remain bounded by zero and 0·1, the average maxima of V, W are up to six times the maximum of U and the relative change from the entrance conditions is increased, as is the rotation, in Figure 5(b–d). An exception is near the corners in Figure 5(c). The edge effects are clearly accentuated here. Figure 5(d) once more hints at linear growth of D within the bend and no growth thereafter, as well as presenting a grid-refinement study for this high-amplitude case. The refinement supports the general numerical accuracy (and ties in with the later analysis).

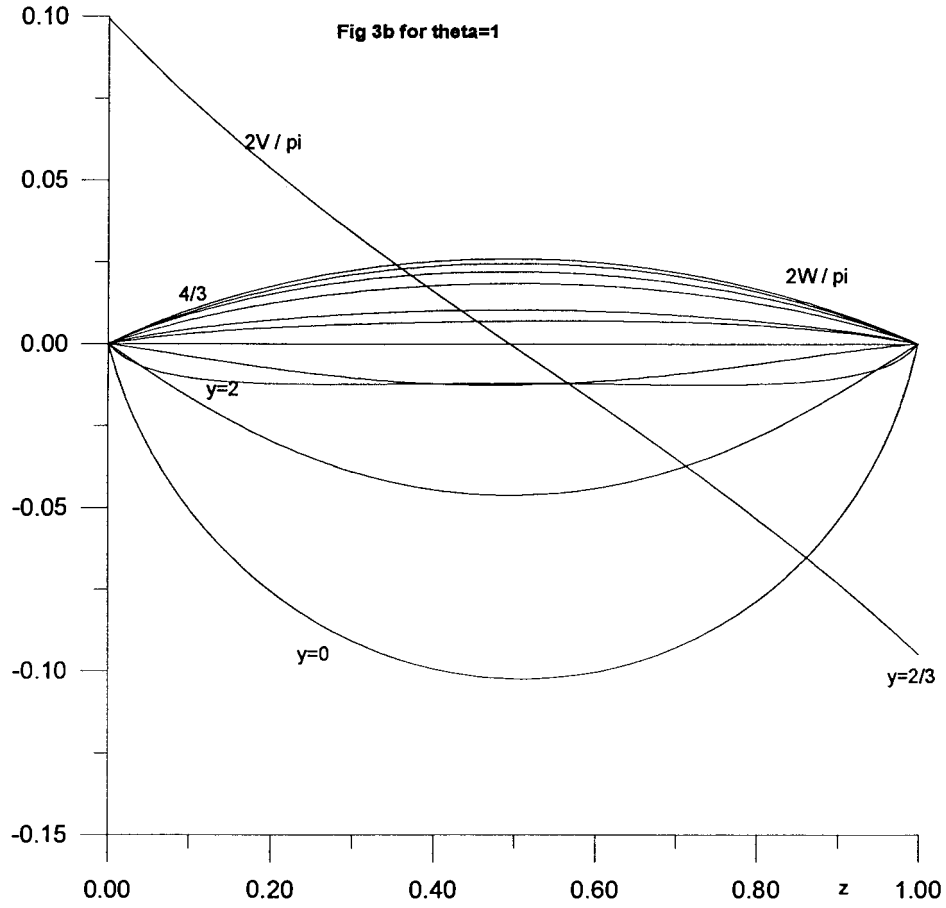

Figure 3. Continued.

Solutions were also computed for certain smooth cross-sections, in order to generalize the applicability as well as to avoid any singular responses associated with corners. The smooth shapes were set by transforming conformally from the above rectangle, adopting the map

$$\zeta = \sum_{n=1}^{4} \left[\left(\bar{\zeta} - \bar{\zeta}_n \right)^2 + 2q \mathrm{e}^{\pm \mathrm{i}\sigma} \right]^{1/2} - \mu \bar{\zeta}. \tag{3.6}$$

Here $\zeta \equiv y + \mathrm{i}z$, $\bar{\zeta} \equiv \bar{y} + \mathrm{i}\bar{z}$ are complex coordinates, while $\bar{\zeta}_n$ for $n = 1$ to 4 signify the four mapped corner points and the signs in (3.6) are chosen such that the eight branch points associated with the square roots lie outside the flow region and geometrical symmetry is preserved. The corresponding eight branch cuts are also taken outside. The real constants σ, μ are adjusted to make the complex derivative $\mathrm{d}\zeta/\mathrm{d}\bar{\zeta}$ vanish at one corner and hence, by symmetry, at all corners. This ensures that the shape in the $y - z$ plane is smooth, free of any corners, as in Figure 6(a–c). Then we performed computations in $\bar{y}, \bar{z}$ rectangular coordinates using a version of the earlier approach modified to account for the modulus of the complex derivative and other mapping quantities appearing in the transformed governing equations. The different cross-sectional shapes obtained from different values of the real constant q and the main flow properties, which yield the same trends as for the rectangular section, are

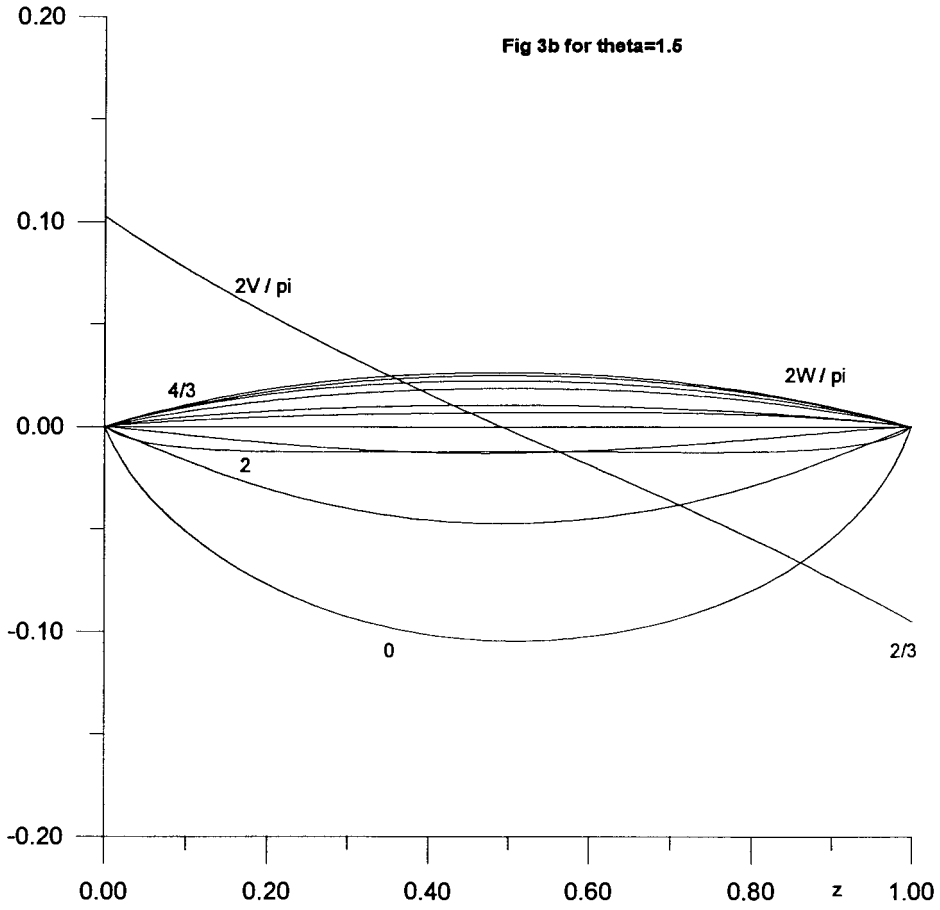

Figure 3. Continued.

presented in Figure 6(a–d). These bent smooth-duct flows have entrance conditions imposed as in (3.5) but with $\bar{y}, \bar{z}$ replacing y, z.

4. General flow properties

Most of the following properties hold for arbitrary cross-sections of duct and arbitrary input conditions, with typically order-one angles θ_1 being turned through (as in the main industrial applications). The flow solution in the bend depends on both the amplitude and the form of the input flow. Thus a simple exact solution for all θ has the component U being an arbitrary function of z and V, W, R, ψ being zero, which corresponds to continued one-dimensional motion, with the pressure response p_1 then being 2Γ multiplied by the integral of U with respect to z. It is clear from the properties below, however, as well as from the earlier numerical results, that such a simple solution is atypical.

Suppose that the inertial effects are comparatively small, this being due to low entrance swirl and/or θ_1 small and/or α small for example. Then to a first approximation, given that the characteristic U value is of order unity and V, W are not large, (2.1b) implies that U remains as $U_I(y, z)$ and so, when V_I, W_I are zero, (3.1) yields the vorticity response

$$R \approx 2\Gamma\theta\partial U_I/\partial y. \tag{4.1}$$

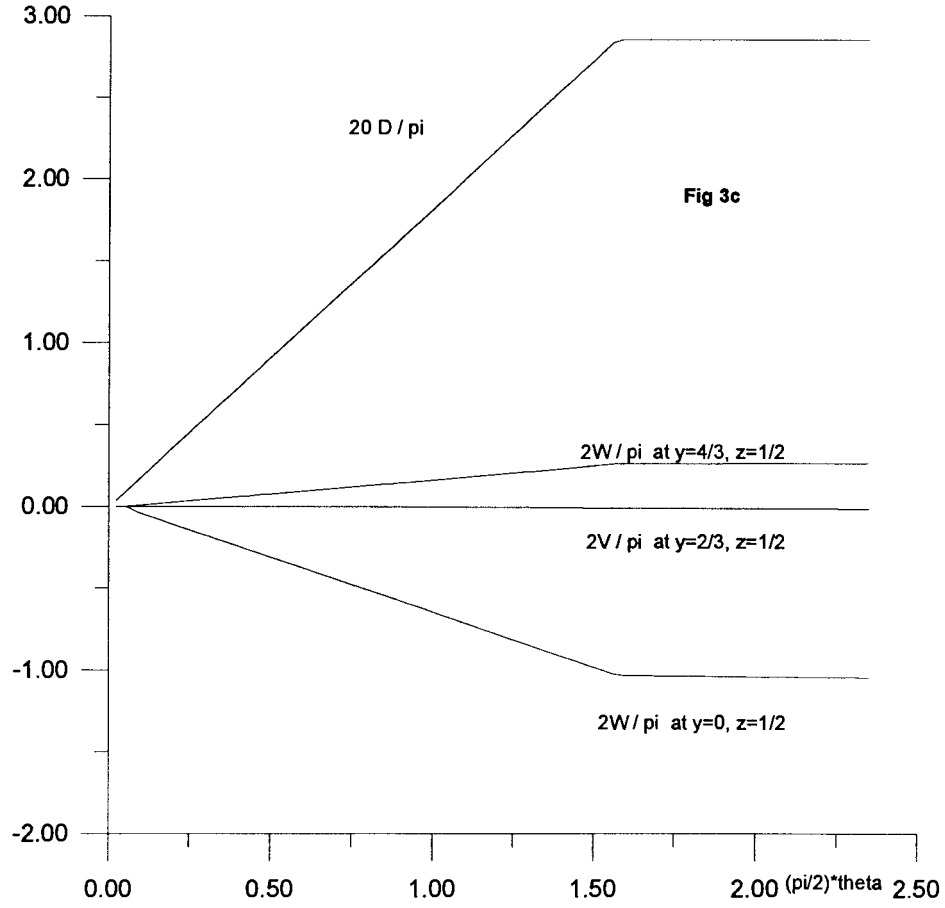

Figure 3. Continued.

For the case of U_I in (3.4) in a rectangular 1-by-2 duct the response (4.1) with (2.4), (3.2) gives the prediction

$$[R, \psi, V, W] \sim 2c\Gamma\theta[2(d_1 + d_2), \quad d_1 d_2, \quad (1 - 2z)d_1, \ 2(y - 1)d_2] \tag{4.2}$$

where $d_1 \equiv y^2 - 2y, \quad d_2 \equiv z^2 - z$. This agrees well with the computational results of Section 3, as is anticipated in Figure 2.

The process indicated above, of V, W essentially driving the evolution of U through (2.1b), which then produces the shear $\partial U/\partial y$ to drive the vorticity R evolution (through (3.1)), which then controls ψ, V, W (through (3.2), (2.4)), and so on, continues in principle for all θ within the bend, at any values of the parameters θ_1, α and input velocity profiles, *i.e.* in the general nonlinear inertial case. It applies for all the computations described in Section 3, the majority of which have U_I dependent only on y and without any symmetry in y.

When θ_1, α and the input conditions are of order unity, the flow problem is largely a numerical one of course, but there are a few useful general properties. First, for a uniform cross-section of duct a double integration of (2.1b) in y, z over the cross-section and application of Green's theorem show that

$$p_0 \equiv 0, \tag{4.3}$$

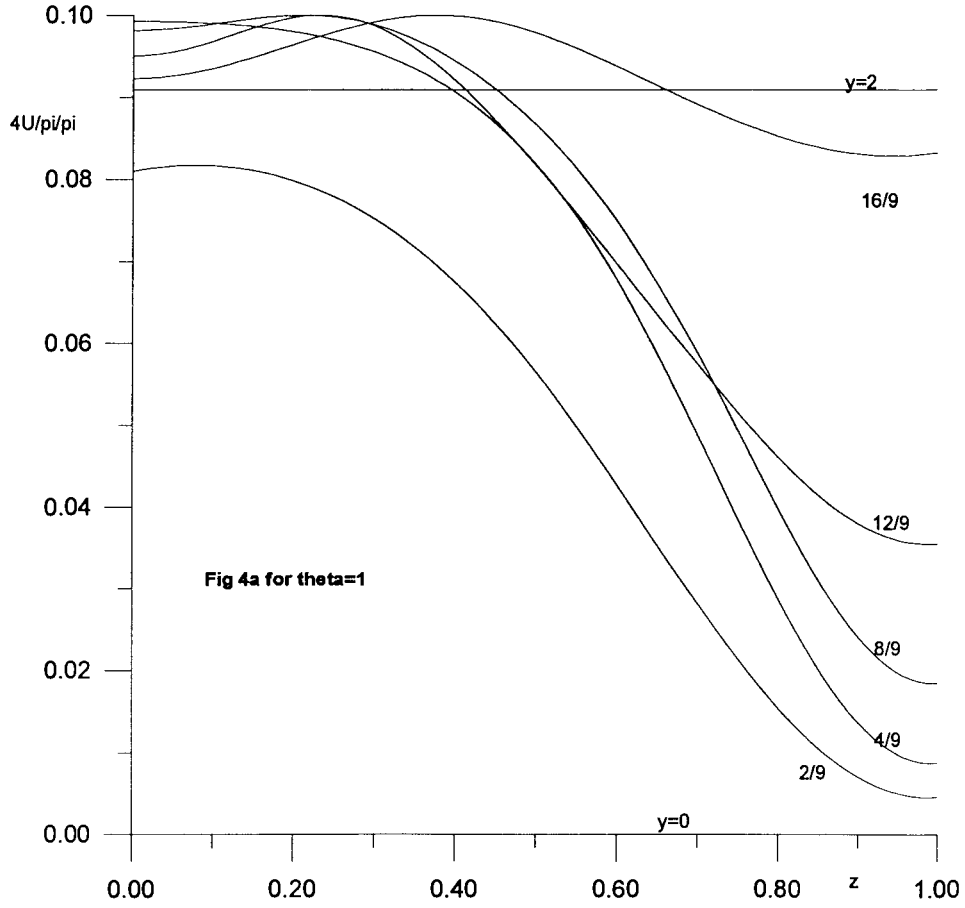

Figure 4. As Figure 3 but the input swirl velocity has $c_2 = 3\pi/2$. (a) $4U/\pi^2$ profiles at $\theta = 1,\ \theta = \frac{3}{2}$. (b) $2V/\pi, 2W/\pi$ profiles at $\theta = 1$. (c) $2R/\pi$ profiles at $\theta = 1,\ \theta = \frac{3}{2}$. (d) has D, and W along $(y, z) = (0, \frac{1}{2})$, versus $\pi\theta/2$.

since (2.3a,b) hold. Second, (2.1b) with (4.3) indicates that U is conserved along streamlines, so that

$$U \text{ is } O(1) \text{ for all } \theta, \tag{4.4}$$

assuming that the input component U_I is of order unity. Third, a double integration of (3.1) in y, z gives the relation

$$\frac{\mathrm{d}}{\mathrm{d}\theta}\left[\iint R\,\mathrm{d}y\,\mathrm{d}z\right] = 2\Gamma \int (U_r - U_\ell)\,\mathrm{d}z \tag{4.5}$$

between the total integrated vorticity evolution and the left (ℓ) and right (r) side values of U induced on the duct boundary at a fixed z.

The relation (4.5) is very helpful. It agrees with (4.1), (4.2) for small inertial forces. It also holds for any finite inertial case however due to cancellations in the nonlinear inertial contributions. The computational results in Section 3 for both rectangular and smooth cross sections tend to confirm this result for all the parameter values studied and indeed (4.5) can

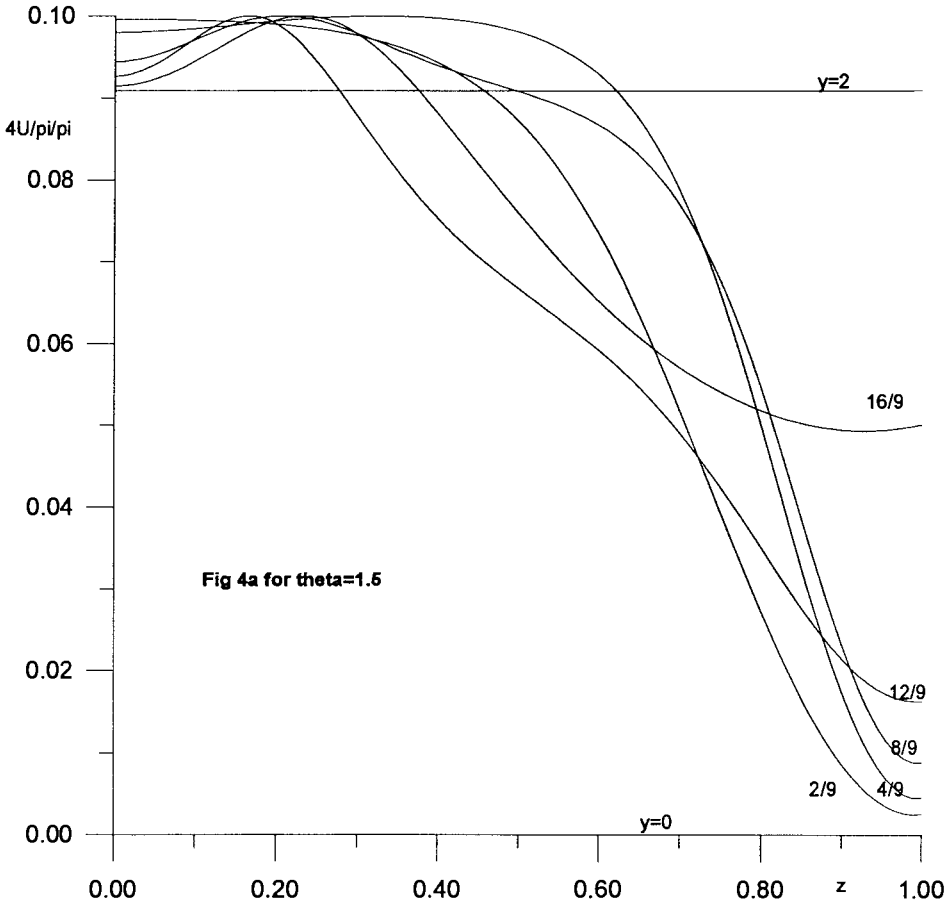

Figure 4. Continued.

be treated as a valuable check on the computational accuracy. Further use is made of (4.5) below.

Fourth, for general $O(1)$ values of the inertial forces we consider the motion downstream of the bend as θ increases. It seems clear from the computational results supported by (4.5) again with zero Γ that the streamwise vorticity R tends to a nonzero steady state $R_\infty(y, z)$ say in general as $\theta \to \infty$, while the streamwise velocity U tends to a $U_\infty(y, z)$ form. The downstream distributions R_∞, U_∞ satisfy (2.1b), (3.1), (3.2) with zero θ-dependence and zero Γ, and hence are de-coupled, and they appear to be arbitrary in that they are determined by the upstream integrated bend effects. It is noteworthy that the influence of the bend on the cross-plane flow (a flow which may be zero before the bend) does not peter out far downstream on the present scales.

Finally here the flow behaviour near a corner requires discussion, in the light of the earlier numerical work. The following suggests that a singular response occurs in general. Suppose that for θ of order unity the vorticity behaves in the form

$$R \sim s^{-n} \tag{4.6a}$$

at small distances s from the corner, where the unknown power n is assumed positive. Then we have from (2.4),(3.2) that $V, W \sim s^{1-n}$. So along one straight side, say where z is constant

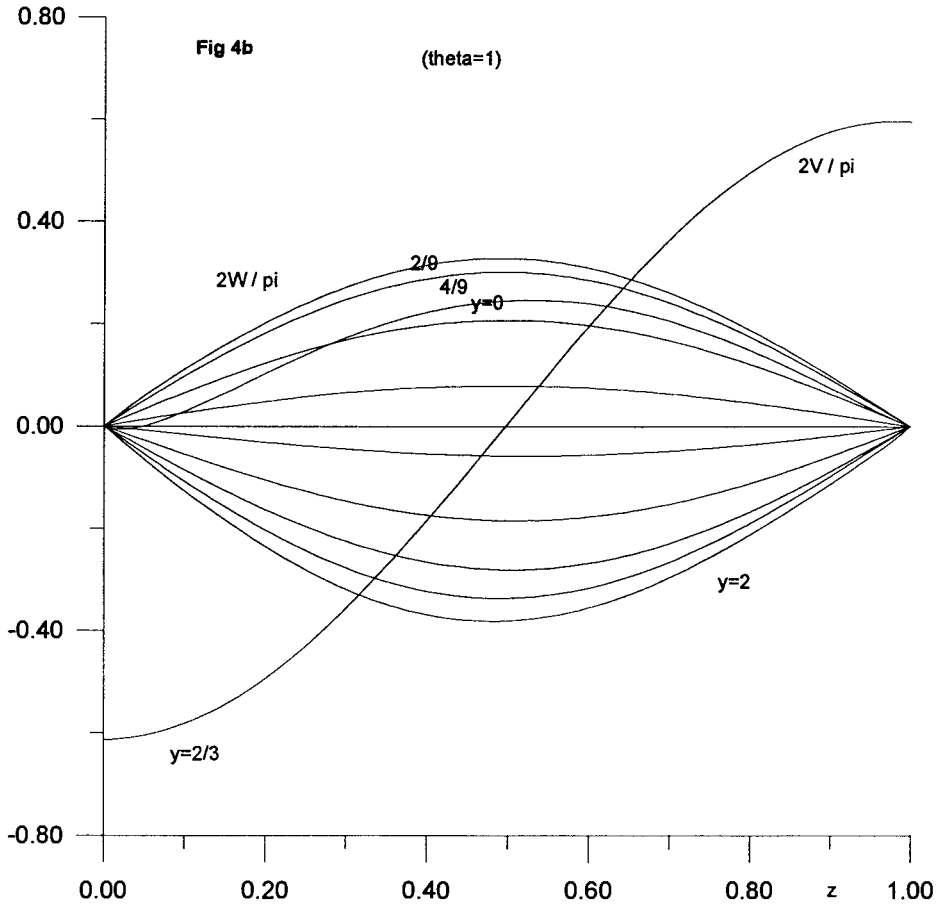

Figure 4. Continued.

and y is tending to zero, (2.1b) gives $\partial U/\partial\theta$ balancing $n^{-1}y^{1-n}\partial U/\partial y$ essentially, and in consequence U is a function of $\theta + y^n$ locally. If the input condition is taken as $U = y$ at $\theta = 0$ for instance, then $U^n = \theta + y^n$ thereafter, yielding $2\partial U/\partial y$ as

$$2y^{n-1}(\theta + y^n)^{\frac{1}{n}-1}. \tag{4.6b}$$

That leaves R in (3.1) satisfying the same balance as U above but forced by (4.6b), along the same side locally. If the input R is zero it follows that the local solution for $\theta > 0$ is

$$R \propto= \frac{2n}{(2n-1)}(\theta + y^n)^{\frac{1}{n}-1}\left\{y^{2n-1} - (\theta + y^n)^{2-\frac{1}{n}}\right\}, \tag{4.6c}$$

provided $n \neq \frac{1}{2}$. The behaviour $R \sim y^{2n-1}$ from (4.6c) is consistent with the original form (4.6a) (here $y = s$) if

$$n = \tfrac{1}{3}, \tag{4.6c}$$

justifying the assumption that n is positive. It is interesting that, as streamlines accumulate near the corner, according to the above, U is not constant there, despite the vanishing of V, W, and that a similar treatment holds along any radius from the corner, suggesting an extension of (4.6a) and related quantities to include azimuthal dependence locally. The nonlinear trend

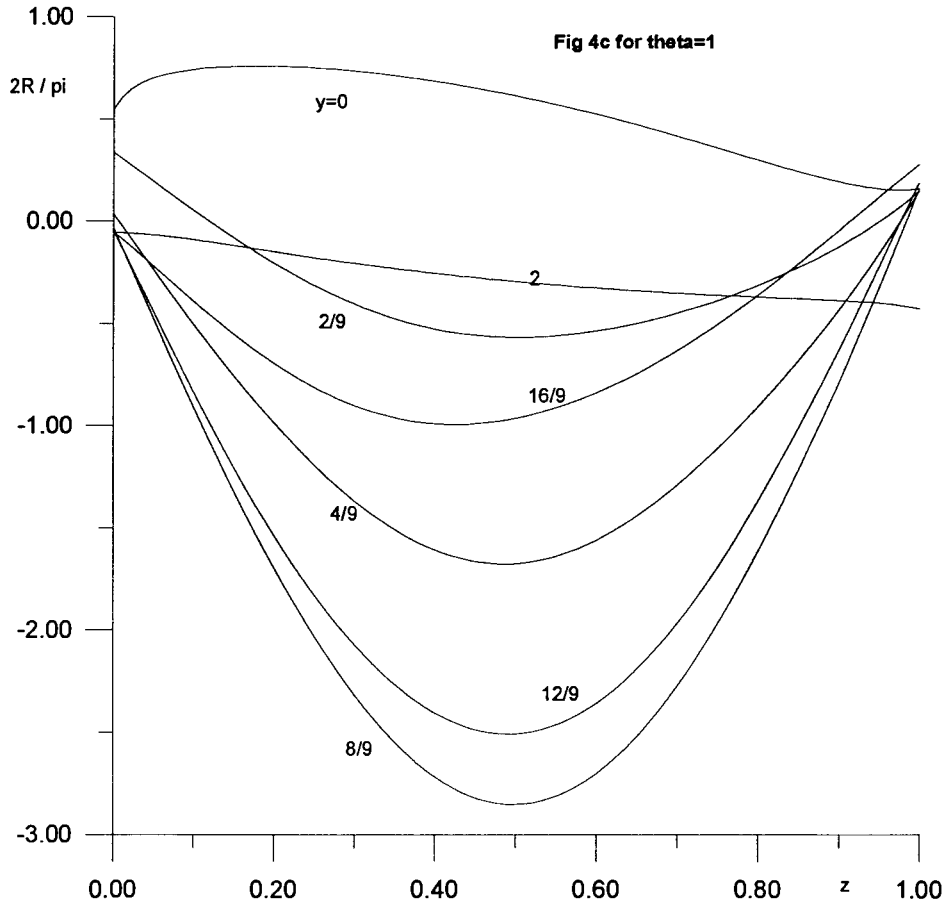

Figure 4. Continued.

indicated by (4.6a–d) near a corner agrees with a small θ solution and it seems to be in line with the computational results for a rectangular cross section.

Further inertial and other effects are discussed in Section 6, after the investigation of swirl effects in the next section.

5. Small and large swirl effects

The influence of the swirl present upstream is of particular interest for practical as well as theoretical reasons; the practical reasons concern valves, imperfections and wall roughness upstream as discussed in detail in the introduction with regard to the industrial setting.

5.1. SMALL SWIRL

For relatively small swirl at the entrance and beyond, the U Equation (2.1b) with (4.3) is dominated by $\partial U/\partial\theta$ being zero, so that U remains as $U_I(y, z)$ to leading order. This is similar to (4.1)–(4.2), as is the balance $\partial R/\partial\theta \approx 2\Gamma\partial U/\partial y$ from (3.1). Hence the weakly nonlinear result

$$R = (\partial W_I/\partial y - \partial V_I/\partial y) + 2\Gamma\theta\partial U_I/\partial y \tag{5.1}$$

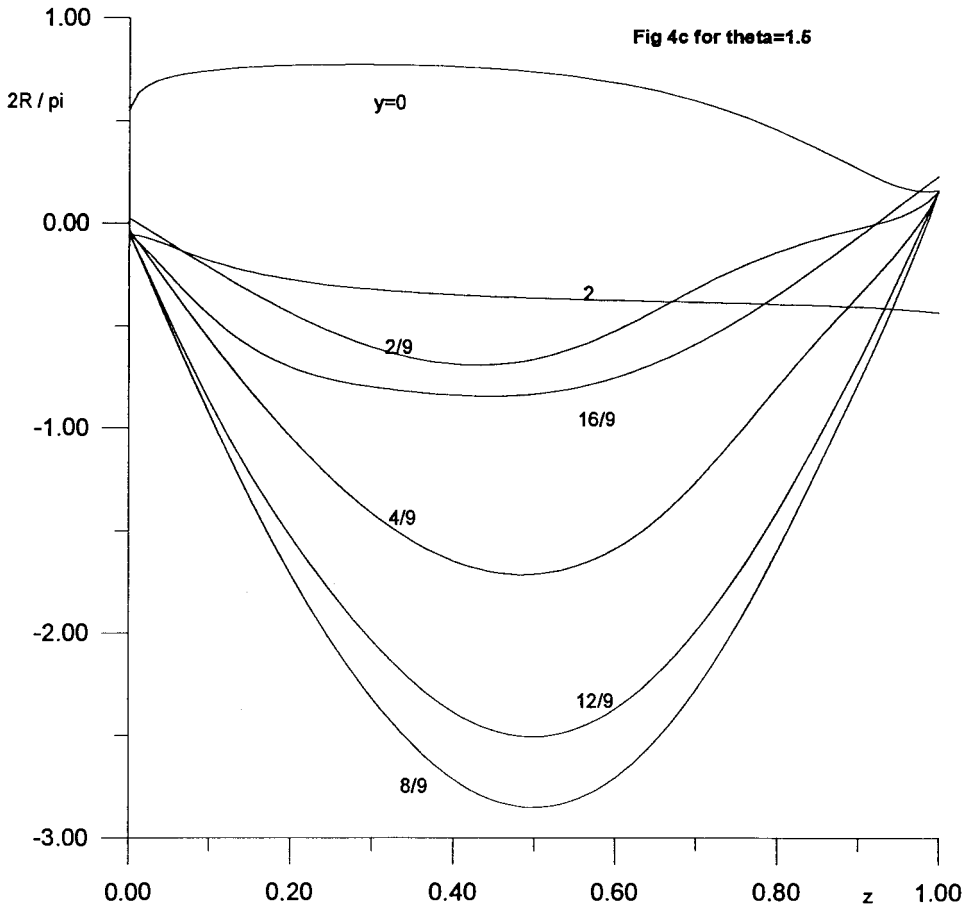

Figure 4. Continued.

follows, showing explicitly a linear growth of the streamwise vorticity in line with the general nonlinear property (4.5). The result (5.1) usually continues for the entire bend since $0 < \theta < 1$ there, with exceptions arising only if another parameter has an extreme value; comparisons with Figures 2,3 are in keeping with this result.

5.2. LARGE SWIRL

For relatively large swirl, on the other hand, there is a strongly nonlinear effect. Here again (4.5) is of interest, combined with (4.4). If the swirl velocities are large, of order Δ say, then the first substantial response occurs over the short scale $\theta = \Delta^{-1}\theta^*$ with θ^* of order unity and

$$R = \Delta R_0 + R_1 + \Delta^{-1} R_2 + \cdots , \tag{5.2a}$$

$$U = U_0 + \cdots , \tag{5.2b}$$

along with expansions for V, W similar to (5.2a), where R_0, U_0 and so on are of order unity. So R_0, V_0, W_0, U_0 satisfy the original governing equations but without the centrifugal term $2\partial U/\partial y$, leaving the streamwise and cross-plane flows decoupled at leading order. The dominant flow solution therefore equilibriates downstream at large θ^*. In the cases of Figures 4,5 in

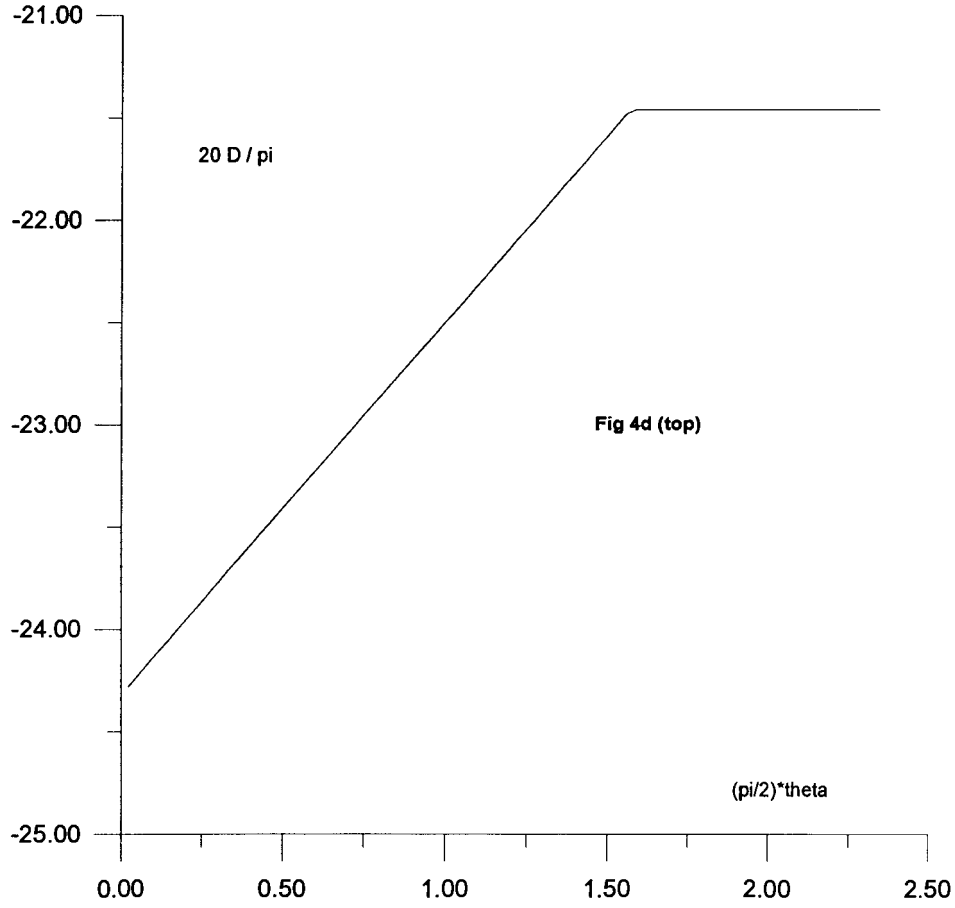

Figure 4. Continued.

fact the input conditions are such that the dominant solution is in equilibrium immediately. At higher order, however, R_2 is driven both by $\partial R_2/\partial\theta^*$ and inertial forces balancing $2\Gamma\partial U_0/\partial y$. Hence integration over the cross section gives

$$\frac{\mathrm{d}}{\mathrm{d}\theta^*}\left[\iint R_2 \mathrm{d}y\,\mathrm{d}z\right] = 2\Gamma\int (U_{0_r} - U_{0_\ell})\,\mathrm{d}z. \tag{5.3}$$

Downstream, in view of the equilibration above in which U_0 tends to an $0(1)$ form independent of θ^*, (5.3) implies that

$$R_2 \propto \theta^* \text{ as } \theta^* \to \infty. \tag{5.4}$$

This is again in line with (4.5).

The behaviour (5.4) shows that inertial effects continue to dominate downstream, from (5.2a,b). The fluid spins more rapidly in the cross section, as the three-dimensional streamlines have slopes $\mathrm{d}y/\mathrm{d}\theta = V$, $\mathrm{d}z/\mathrm{d}\theta = W$ which are comparatively large. The slight growth in vorticity inferred from (5.4) also agrees with the computational solutions in Figures 4 and 5. If θ_1 and other parameters are not particularly extreme, then the growth (5.4) is insufficient to disturb the expressions in (5.2a,b), which in essence describe the entire bent-duct motion.

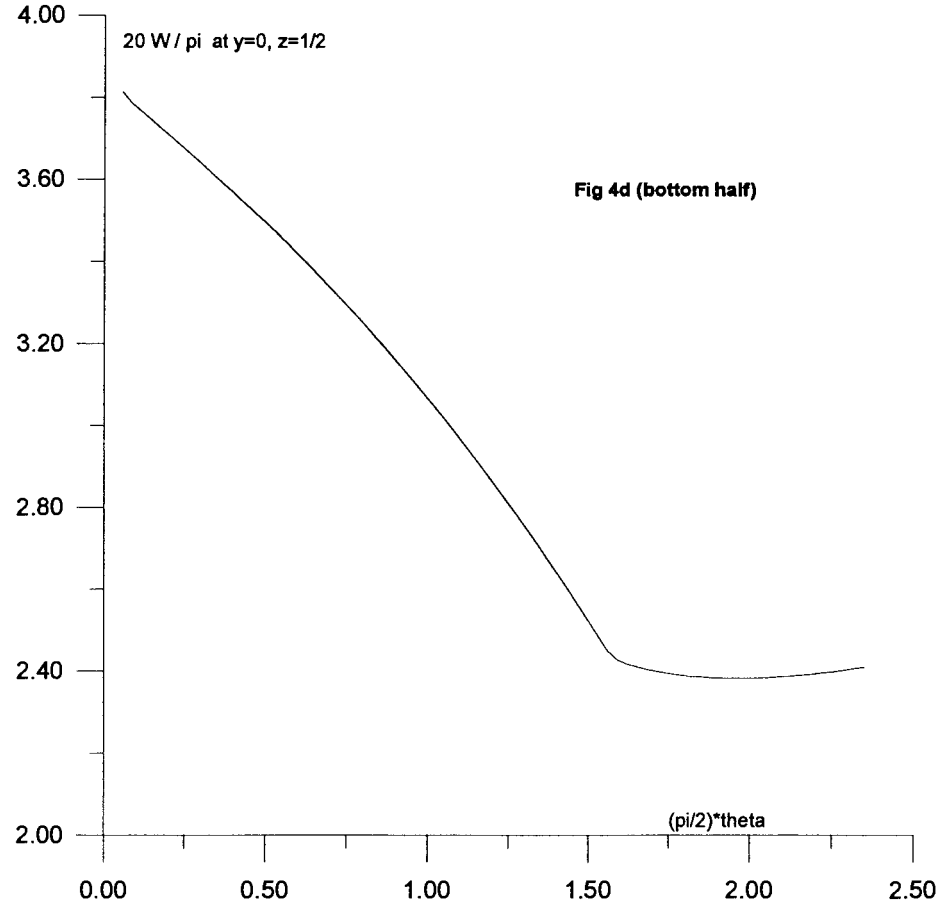

Figure 4. Continued.

Under sufficiently extreme (but not uncommon) conditions a second stage occurs when $\theta = \Delta\Theta$ is large and of order Δ but expressions of the form (5.2a,b) re-apply. These yield the quasi-planar balances

$$V_0 R_{0y} + W_0 R_{0z} = 0,\ V_0 U_{0y} + W_0 U_{0z} = 0 \tag{5.5a,b}$$

from (2.1b),(3.1),(4.3). The solution has the scaled vorticity R_0 being $f(\Theta)R_\infty(y,z)$ with R_∞ determined by matching with the previous stage and depending on the stream function but with f unknown. Then at higher order $\partial R_0/\partial\Theta$ appears together with further inertial terms and $2\partial U_0/\partial y$, and so upon cross-sectional integration, as with (4.4), (4.5), the rate of change of the R_0 integral with respect to Θ must remain $O(1)$. It follows that $f(\Theta)$ becomes linear in Θ. Thus the linear growth of the vorticity with θ continues. Its general form is

$$R \sim \theta \bar{R}_0(y,z), \qquad U \to \bar{U}_0(y,z) \tag{5.6}$$

and likewise for V, W, ψ if θ can become sufficiently large with Γ still nonzero. In a more precise argument here, a fluid particle on any flat side of a rectangular duct must remain on that side, from (2.3a),(4.6) and the presence of cross-flow stagnation points at the duct corners, and so in the cases in Section 3 where U_I is independent of z for example the streamwise velocity U has to remain uniform on the sides $y = 0, y_1$ throughout the bend, from (2.1b),(4.3). So

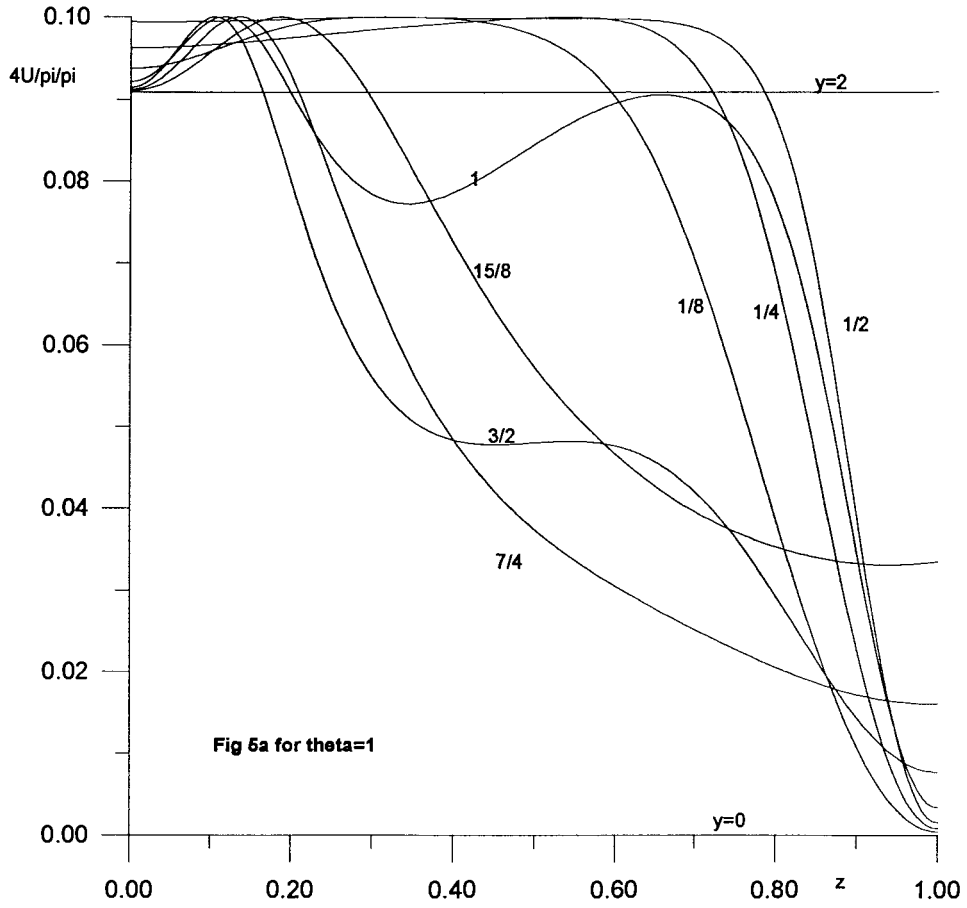

Figure 5. As Figure 3 but with input swirl parameter increased still further, to $c_2 = 3\pi$. (a) $4U/\pi^2$ profiles at $\theta = 1,\ \theta = \frac{3}{2}$. (b) $2V/\pi,\ 2W/\pi$ profiles at $\theta = 1$. (c) $2R/\pi$ profiles at $\theta = 1,\ \theta = \frac{3}{2}$. (d) gives D versus $\pi\theta/2$ from three different numerical grids: (i) coarse, 61×61 in cross-plane; (ii) medium, 121×121; (iii) fine, 161×161.

U_r, U_ℓ in (4.5) are then constants, and in general different constants, which can be evaluated directly from the input profile U_I and make the right-hand side of (4.5) an explicit constant for all θ. Supposing also that the cross-plane flow eventually swirls only clockwise, say, we see that U must then tend towards uniform values on the two other sides $z = 0,\ z_1$, again from (2.1b),(4.3), these values being equal to those on $y = y_1,\ 0$, respectively, and similarly anticlockwise swirl interchanges the values. This argument generalises as indicated in Figure 7 (which shows the large-θ form for a smooth input U_I, along the left, top, right and bottom edges of a 3 by 1 rectangle) and points to an approach towards discontinuities in the U distribution at certain of the duct corners, in line with the computations. The argument also fixes precisely the r, ℓ values in (4.5) downstream and hence the growth rate in (5.6).

In addition to (5.2a,b), (5.5a,b),(5.6) which hold in the core of the motion, thin edge layers are generated near the duct boundary, to allow for significant θ variation. Their typical thickness is of the order $\exp(-\theta^2)$ in order to balance the operators $\partial/\partial\theta$ and, from the tangential cross-plane component, $\theta W_0 \partial/\partial z$ near the sides $y = 0,\ y_1$ for example, where $W_0,\ z$ are usually of order one. The same small exponential scale is implied in the trend to a discon-

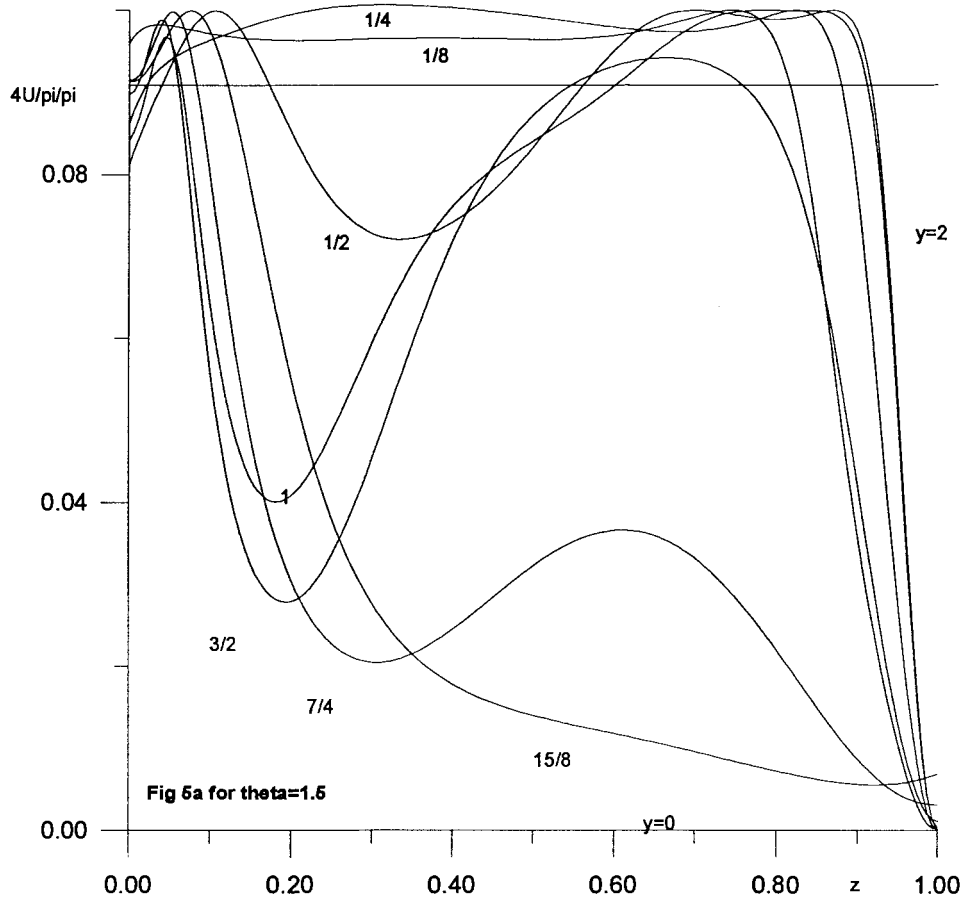

Figure 5. Continued.

tinuous U distribution in Figure 7, as well as in the core centre(s) where V_0, W_0 vanish. The edge layers bring in substantial $\partial/\partial\theta$ evolutionary contributions from (2.1b),(3.1) as opposed to the quasi-straight inertially dominated form (5.5a,b) in the core. This description for bent flows downstream, and the emergence of thin edge layers as well as the growth in (5.6) with θ associated with increasingly high swirl, explains the numerical difficulties for extreme cases in Section 3. (After the bend the linear increase in (5.6) ceases of course).

6. Further discussion

6.1. VARYING THE TURNING ANGLE, ENTRANCE VELOCITIES AND CURVATURE OF THE BEND

Here we begin by considering the influences of varying (i) θ_1,(ii) ϵ,(iii) a separately, which are related to the influences described in the previous section.

Thus (i) a small turning angle θ_1 makes the normalized input velocities U_I, V_I, W_I small, of successive orders $\theta_1^2, \theta_1, \theta_1$, if a, ϵ and the real velocity perturbations $\tilde{U}_I$, $\tilde{V}_I$, $\tilde{W}_I$ are kept fixed. Assuming U, V, W to take the same successive orders shows that the inertial forces then are again low although the centrifugal effect is diminished compared with that in (5.1).

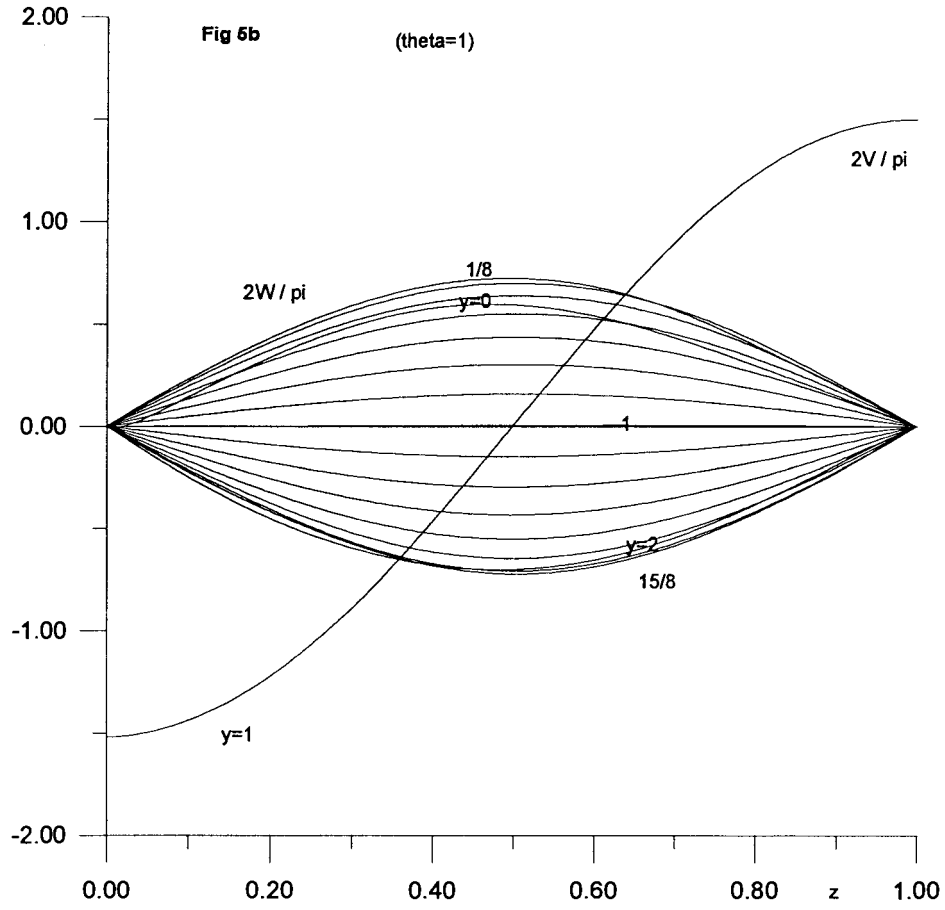

Figure 5. Continued.

Conversely a large value of θ_1, for a highly coiled duct, requires renormalizing U, V, W by factors θ_1^2, θ_1, θ_1 and using the original angle $\tilde{\theta}$ at first. This reinstates the nonlinear governing equations but subject to 0(1) entrance conditions, while the $\tilde{\theta}$ range is semi-infinite in effect. Domination by high swirl as in (5.2a)–(5.6) can be expected to emerge downstream.

(ii) Reduction or increase of the input perturbation velocities from the straight duct downstream is reflected simply in ϵ, and hence α, becoming smaller or larger in turn.

(iii) The same applies if the radius of curvature a is decreased or increased, respectively, provided other conditions are maintained. Both (ii),(iii) correspond to extremes of the parameter α, then, which shows itself only in the input velocities being proportional to α.

The regime of small α values is equivalent to those for small swirl described in Section 5.1 and small inertia in Section 4.

Similarly, large-α effects appear as for large swirl in Section 5.2. Provided that U, V, W, R are all comparable and scale as α, the short range $\theta \sim \alpha^{-1}$ is indicated first, where the centrifugal force is secondary and so the primary flow solution equilibrates. By contrast the contribution of order unity to R grows linearly in $\alpha\theta$, due to (4.5). In consequence an inertial growth takes place on the longer range where θ is of order one exactly as in Section 5.2. A slightly different short-range initiation occurs if the entrance swirl velocities are much less than the streamwise velocity perturbation, such that U, V, W scale with α, $\alpha^{1/2}$, $\alpha^{1/2}$ in turn,

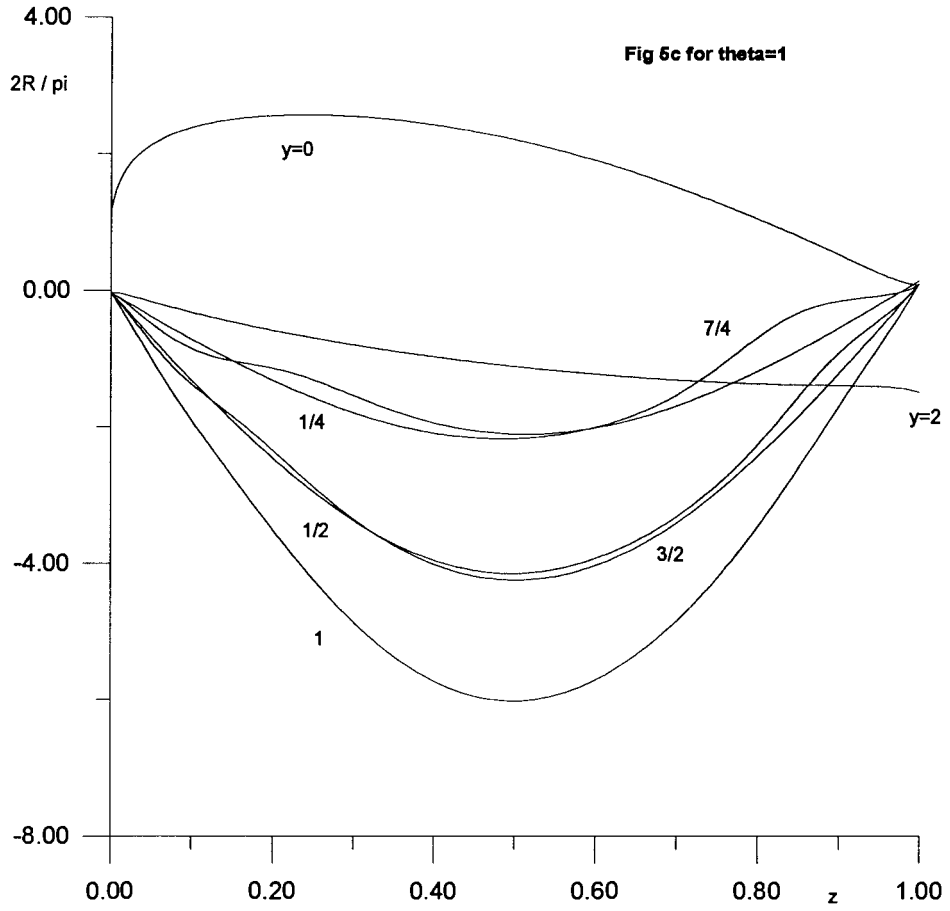

Figure 5. Continued.

since then θ scales with $\alpha^{-1/2}$ instead, leaving the full nonlinear equations intact. This case retrieves the large-θ_1 properties discussed in (i) at the start of this subsection.

6.2. Related points

This work has focused primarily on swirl effects, as discussed especially in Section 5; the alterations to other conditions in Section 6.1 tend to support that focus. Dependence on the parameters α, θ_1 is clearly present also, due to the factors in Section 2 and bearing in mind that the original vorticity and stream functions are $(R, \psi)/(\alpha\theta_1)$. The present study, however, indicates strong dependence on the form of the input velocities, including swirl, at the entrance to the bend. Likewise, whether for smooth general shapes of cross section or the rectangular ones with their extra, but localised, flow responses near each corner, the central feature (inferred from (4.5) with (4.4)) of unbounded linear growth in the total streamwise vorticity accentuates the importance of the induced swirl.

The central points (a)–(e) of the industrial setting given in the introduction, to repeat, emphasize new features in themselves. Viscous effects in particular are neglected on the grounds that laminar flow would remain attached over the short time scales of industrial concern, while turbulent (plug) flow would not be prone to separate anyway. Exceptions to this can occur in

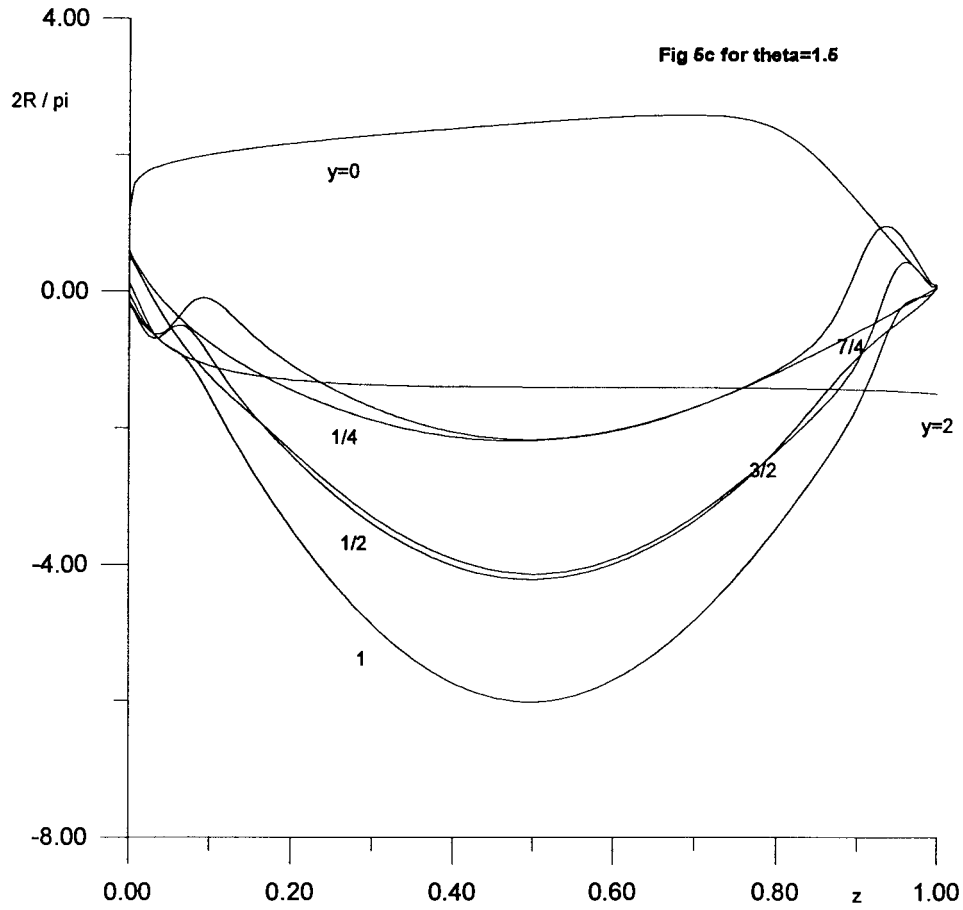

Figure 5. Continued.

extremes, of course, such as at large times or very close to a corner or a wall or very far downstream: compare with Section 4. Again direct experimental comparison is lacking and in a sense theory must take the lead, as hinted at in the introduction. Comparing with [20]'s brief comments on relevant experiments and [33]'s turbulent-flow results for square ducts, we find that imbedded helical motions and doubly peaked axial velocity profiles can occur as in experiments. Theoretically, these depend on the input conditions, as does the direction of the cross-sectional flow (see also [33]) under centrifuging and radial pressure gradient. We also refer forward here to the fourth paragraph below.

The enhanced impact for larger ϵ (*i.e.* for increased input velocity perturbations) is clearly sensible physically, whereas the impact of increasing the bend radius a alone, namely an enlargement of the swirl (see Section 6.1), is a surprising property at first glance. The latter is due, however, to the corresponding increase in the bend length for a given turned angle θ_1. If we consider instead a given length of bend, then we have $\alpha\theta_1$ being fixed along with a given $(\tilde{U}_I, \tilde{V}_I, \tilde{W}_I)$ input, which implies the orders $(\theta_1, 1, 1)$ for (U_I, V_I, W_I) in general. So here a small turned angle θ_1 immediately yields a dominant swirl effect with negligible centrifuging as before, while the case of large θ_1 is equivalent to that of large α also described previously. These alterations for a fixed bend length thus make good physical sense.

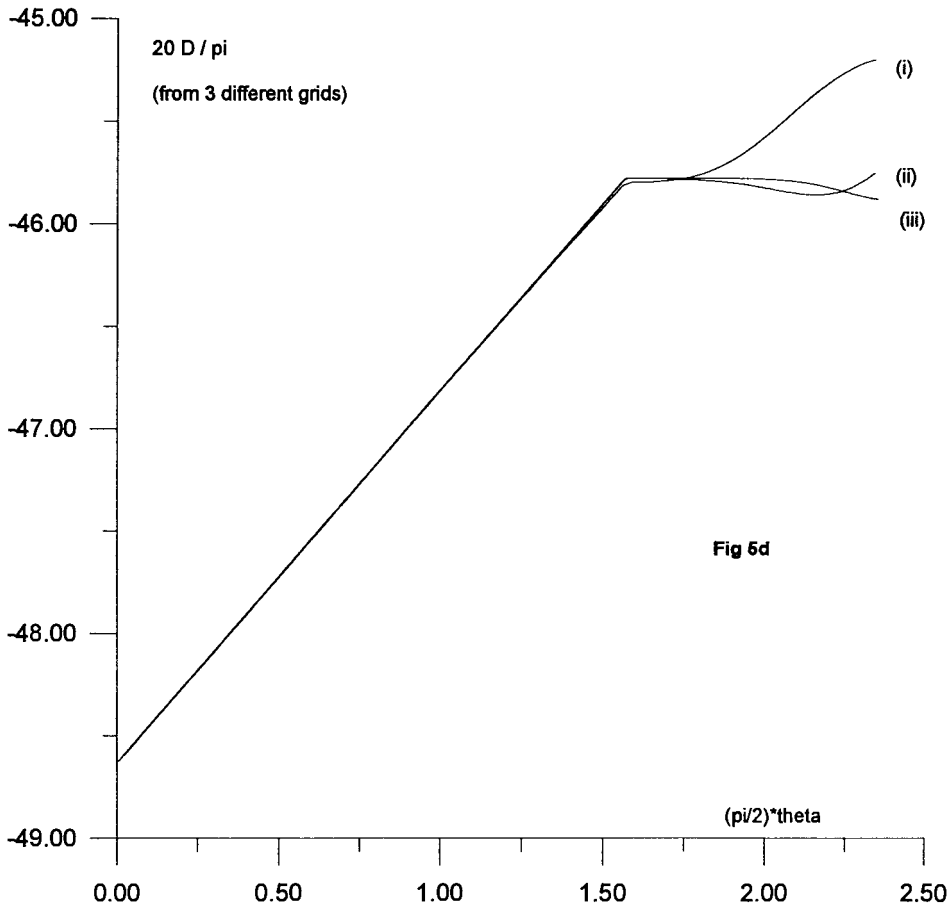

Figure 5. Continued.

The unsteady counterpart of the present work has a scaled operator $\partial/\partial t$ added to $\partial/\partial\theta$ in the governing Equations (2.1b),(3.1) and so essentially leaves the present findings unchanged in a forward-moving frame. Similarly other shapes of bend and duct cross section are to be covered by a generalization of the current approach.

The even more nonlinear case, however, where in effect $\partial/\partial\theta$ is replaced by $U\partial/\partial\theta$, $2\partial U/\partial y$ by $U\partial U/\partial y$, and $\partial U/\partial\theta$ is added to the continuity balance, needs further study, particularly in terms of a likely breakup singularity arising at a finite θ value. That case loses the feature ((4.4),(4.5)) of unbounded linear growth. It also points to considerable influence on one-dimensional duct-flow analysis. The leading-order influence so far from the cases addressed in the present work is still small except for the extreme conditions mentioned where for example the growth (5.6) holds, sometimes over a relatively short θ-range. The increase in cross-plane inertia resulting from (5.6) tends to lead to the $U\partial U/\partial\theta$ case, altering the total streamwise velocity profile rather than a perturbation as before. Further study on this is being conducted by Mr. P.L. Wilson at UCL, linked with Sortex Ltd., along with the inclusion of compressibility.

The above trends also point to the desirability in practice of suppressing the oncoming spanwise and streamwise vorticity, generating input swirl, especially from any imperfections upstream. That suppression tends to reduce both the secondary flow produced by the bend

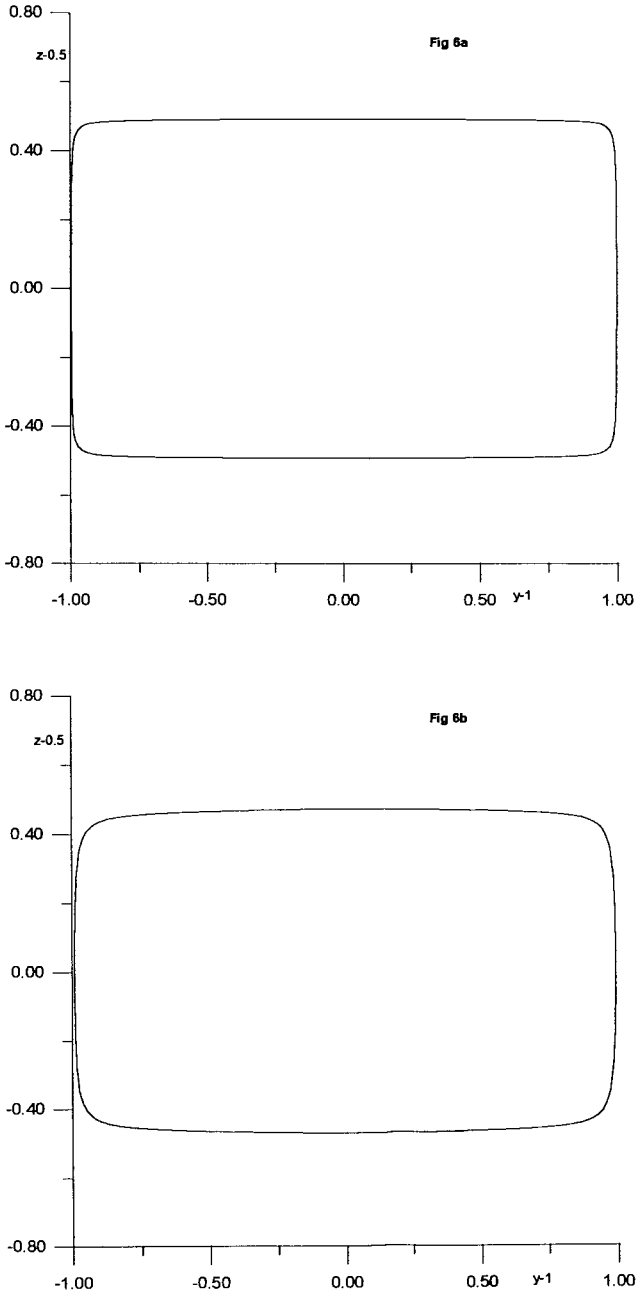

Figure 6. For smooth cross sections, from (3.6). (a–c) Cross-sectional shapes for three values of q (0·005, 0·02, 0.1). (d) The corresponding numerical solutions, giving D versus $\pi\theta/2$.

and its interaction with the streamwise motion. Here the simple weak-inertia results in Sections 4, 5 may well prove the most useful overall as, for a typical bend ratio a of 10 say, those results apply for representative velocity perturbations (ϵ values) up to about 10%. (In [33]'s experiments a is 2·3 and ϵ is 0·28, considerably smaller and larger respectively than the values quoted in the preceding sentence, and indeed [33]'s results also are more indicative of the more nonlinear case of the previous paragraph.) Again, the pressure response in the bend

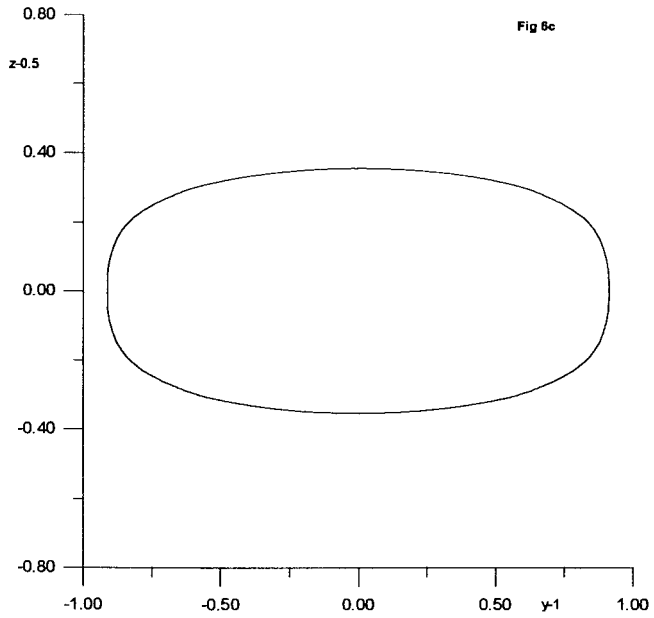

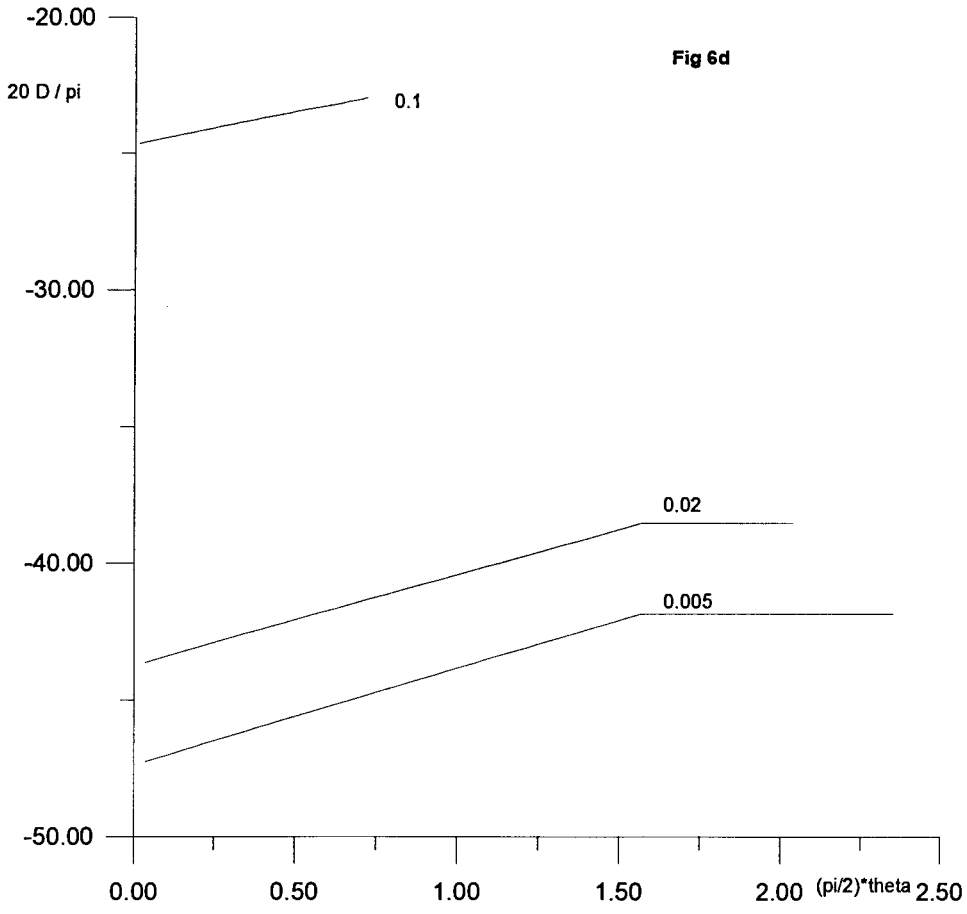

Figure 6. Continued.

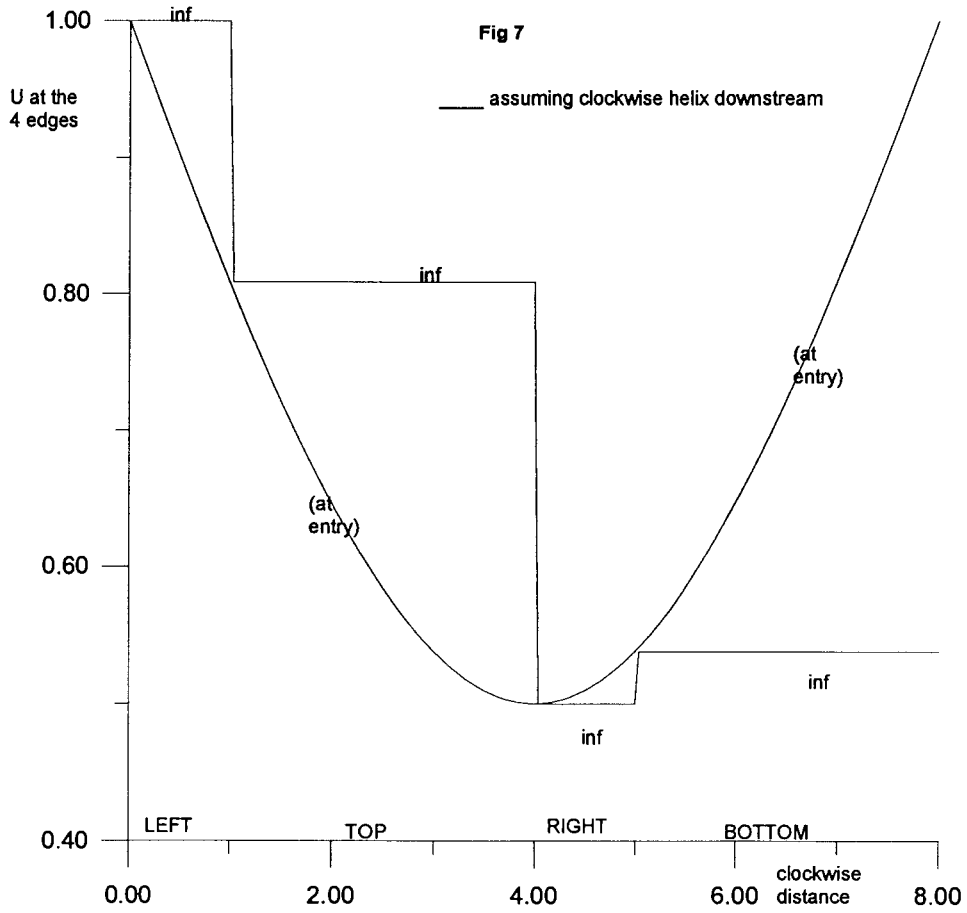

Figure 7. The effect of increasing swirl downstream (Section 5.2) on the edge values of the slip velocity U, for a rectangular cross section; showing the smooth entry condition and the large-θ form (denoted inf) for the four sides of a 3 by 1 rectangle in this case.

is small here because of the vanishing of the leading-order pressure term, in (4.3), owing to the constant duct area. The main response thus rests on the order ϵ^2 contribution p_1 appearing in (2.1c,d), which can be positive or negative. An arbitrary function of θ that can be added to p_1 is determined by higher-order balances involving $U\partial U/\partial\theta, UW$, and so on; compare the nonlinear regime above. The case (4.2) for example yields $p_1 \propto c$, while small and large swirl in Section 5 yield p_1 of order U_I, Δ^2, respectively, and the linear growth (5.6) gives $|p_1| \propto \theta_1^2$, but either sign of pressure is possible at this level. The possibility here of little or no pressure loss in inviscid flow due to short active time scales or turbulence offers an interesting contrast with the pressure losses common in viscous flows. This connects back to the industrial applications.

Acknowledgements

This research arose directly from contacts with Sortex Ltd. of London. Thanks are due to Dr. Sarah Bee, Dr. Mark Honeywood and Dr. Jon Ben of Sortex Ltd. for many related discussions,

to Mr.Phillip Wilson for discussions and pointing out some errors in the original presentation, to the Leverhulme Trust for support (L.L.) and to the referees for helpful comments.

References

1. H. Ito, Friction factors for turbulent flow in curved pipes. *J. Basic Engg.* 81D (1959) 123–134.
2. H. Ito, Pressure losses in smooth pipe bends. *J. Basic Engg.* 82D (1960) 131–143.
3. B.S. Massey, *Mechanics of Fluids* (4th ed). New York: Van Nostrand Reinhold (1992) 376 pp.
4. G.I. Taylor, The criterion for turbulence in curved pipes. *Proc. R. Soc. London* A124 (1929) 243–249.
5. W.R. Dean, Note on the motion of fluid in a curved pipe. *Phil. Mag.* 4 (1927) 208–223.
6. D.J. McConalogue and R.S. Srivastava, Motion of a fluid in a curved tube. *Proc. R. Soc. London* A 307 (1968) 37–53.
7. N. Riley, private communications (1978).
8. W.M. Collins and S.C.R. Dennis, The steady motion of a viscous fluid in a curved tube. *Quart. J. Mech. Appl. Math.* 28 (1975) 133–156.
9. L.-S. Yao and S.A. Berger Entry flow in a curved pipe. *J. Fluid Mech.* 67 (1975) 177–196.
10. F.T. Smith, Steady motion within a curved pipe. *Proc. R. Soc. London* A 347 (1976) 345–370.
11. P. Blennerhassett, *Secondary Motion and Diffusion in Unsteady Flow in a Curved Pipe.* Ph.D. thesis (1978) University of London (1976) 212 pp.
12. S.C.R. Dennis and M. Ng, Dual solutions for steady flow through a curved tube. *Quart. J. Mech. Appl. Math.* 35 (1975) 219–236.
13. M.P. Singh, Entry flow in a curved pipe. *J. Fluid Mech.* 65 (1974) 517–539.
14. K. Stewartson and C.J. Simpson, On a singularity initiating a boundary-layer collision. *Quart. J. Mech. Appl. Math.* 33 (1982) 59–75.
15. F.T. Smith, Fluid flow into a curved pipe. *Proc. R. Soc. London* A 351 (1976) 71–87.
16. R. Ahmad, *Fluid Flow through a Cornered or Bent Pipe.* Ph.D. thesis University of London (1996) 258 pp.
17. W.H. Lyne, Unsteady viscous flow in a curved pipe. *J. Fluid Mech.* 45 (1971) 13–31.
18. K.M. Patil and K. Subbaraj, Arterial bifurcation flows – effects of flow rate and area ratio. In: S.D. Nigam and M. Singh (eds.), *Physiological Fluid Dyn. I.* Madras: ICSU (1985) pp. 81–89.
19. C.G. Caro, T.J. Pedley, R.C. Schroter and W.A.Seed, *The Mechanics of the Circulation*. Oxford: Oxford Medical Pubs. (OUP) (1985) 527 pp.
20. S.A. Berger, L. Talbot and L.-S. Yao, Flow in curved pipes. *Ann. Rev. Fluid Mechs.* 15 (1983) 461–512.
21. C.G. Caro, D.J. Doorly, M. Tarnawski, K.T. Scott, Q. Loy and C.L. Dumoulin, Non-planar curvature and branching of arteries and non-planar type flow. *Proc. R. Soc. London* A 452 (1996) 185–197.
22. J.H. Horlock and B. Lakshminarayana, Secondary flows: theory, experiment, and application in turbomachinery aerodynamics. *Ann. Rev. Fluid Mechs.* 5 (1973) 247–280.
23. J.T. Higginbotham, C.C. Wood and E.F. Valentine, A study of high speed performance characteristics of 90 degree bends in circular ducts. *NACA* TN3696, June 1956.
24. S. Kamiyama, Two dimensional potential theory on flow through a bend of arbitrary profile. *Rept. Inst. High Sp. Mech.* Japan V15 No. 147 (1964).
25. J. Lau, Recalculation of incompressible flow in two-dimensional bends. *Can. Aeron. Space J.* 19 (1996) 21–29.
26. A.C. Hurd and A.R. Peters, Analysis of flow separation in a confined two-dimensional channel. *Trans. ASME, J. Basic Engg.* 92 (1970) 908–917.
27. F.T. Smith, Upstream interactions in channel flows. *J. Fluid Mech.* 79 (1977) 631–655.
28. F.T. Smith and P.W. Duck, On the severe non-symmetric constriction, curving or cornering of channel flows. *J. Fluid Mech.* 90 (1980) 727–753.
29. D.J. Monson, H.L. Seegmiller and P.K. McConnaughey, Comparison of LDV measurements and Navier-Stokes solutions in a two-dimensional 180-degree turn- around duct. 27th Aerospace Sciences Meeting, Jan.9–12, (1989) Reno, Nevada.
30. R. Hirsh, Higher order accurate difference solutions of fluid mechanics problems by a compact differencing technique. *J. Comp. Phys.* 19 (1975) 90–109.
31. L. Li, *Numerical Study of Nonlinear Evolution Equations, using Compact Differencing. Ph.D. thesis* (1998) Univ. of London (1998) 240 pp.

32. L. Li, J.D.A. Walker, R.I. Bowles and F.T. Smith, Short-scale break-up in unsteady interactive layers: local development of normal pressure gradients and vortex wind-up. *J. Fluid Mech.* 374 (1998) 335–378.
33. J.A.C. Humphrey, J.H. Whitelaw and G. Yee, Turbulent flow in a square duct with strong curvature. *J. Fluid Mech.* 103 (1981) 443–463.